https://doi.org/10.5194/egusphere-2022-674
Preprint. Discussion started: 16 August 2022

Glacier Energy and Mass Balance (GEMB v1.0): A model of firn processes for cryosphere research

Alex S. Gardner[1], Nicole-Jeanne Schlegel[1], Eric Larour[1]

[1]Jet Propulsion Laboratory, California Institute of Technology, Pasadena, 91109, United States of America

Correspondence to: Alex S. Gardner (alex.s.gardner@jpl.nasa.gov)

Abstract. This paper provides the first description of version 1.0 of the open-source Glacier Energy and Mass Balance model. GEMB models the ice sheet and glacier surface-atmospheric energy and mass exchange, and firn state. It is a column model (no horizontal communication) of intermediate complexity that includes those processes deemed most relevant to glacier studies with the goal of retaining computational efficiency that can accommodate the very long (thousands of years) spin-ups necessary for initializing deep firn columns and for running sensitivity experiments to characterize model uncertainty on continental scales. The model is one-way coupled with the atmosphere which allows the model to be run off-line with a diversity of climate forcing but neglects feedback to the atmosphere. GEMB provides numerous parameterization choices for various key processes (e.g. albedo, subsurface shortwave absorption, and compaction), making it well suited for uncertainty quantification and model exploration. The model is evaluated against the current state-of-the-art and in situ observations and is shown to perform well.

1. Introduction

The near surface (upper most tens to hundreds of meters depth) energy and mass budget of mountain glaciers, icefields, ice caps and ice sheets (i.e. glaciers) is controlled by complex interactions between clouds, the atmospheric boundary layer, the ice surface, and processes internal to the ice-air matrix (cf. Munro & Davies, 1977; Colbeck, 1982; Wiscombe & Warren, 1980; van den Broeke et al, 1994; Greuell & Konzelmann, 1994). It all starts with the nucleation of supercooled water vapor around impurities in the atmosphere that form highly dendritic ice crystals that become heavy and fall from the atmosphere and deposit on the glacier surface forming a highly reflective, insulative, and low-density surface layer. Over time, ice crystals tend towards a shape that minimizes surface area through vapor diffusion and mechanical breakage, rounding the crystals, reducing reflectance (cf. Brun, 1989; Flanner & Zender, 2016; Gardner et al. 2010) and increasing both density and thermal conductivity (e.g. Calonne et al., 2019). The rate at which the metamorphism takes place depends on both the mean temperature and spatial gradients in temperature (e.g. Herron and Langway, 1980; Anthern et al., 2010). This layer will become buried by successive snowfalls, subjecting it to increasing overburden stress that causes the crystals to slide and compact, further increasing both density and conductivity as the snow transitions to firn. Sliding of crystals tends to control the rate of compaction as the firn approaches a

https://doi.org/10.5194/egusphere-2022-674
Preprint. Discussion started: 16 August 2022

density of ~550 km m^{-3} after which the migration of grain boundaries, through sintering processes, controls the rate of compaction to the point at which the air within the ice matrix becomes sealed off from the surrounding pore space at a density of ~830 kg m^{-3} (cf. Herron and Langway, 1980; Alley, 1987). Beyond a density of 830 kg m^{-3}, compaction is regulated by the compression of the air within the sealed pore space.

Under most conditions, net solar radiation is the largest input of energy for melting of ice (cf. Male and Granger, 1981). The amount of solar energy absorbed is largely governed by the effective grain size of the snow crystals within the top few centimeters of the surface, in combination with the concentration and placement of light absorbing impurities (cf. Gardner & Sharp, 2010; Warren & Wiscombe, 1980). This dependency can create strong feedbacks in the energy balance wherein increased solar input leads to enhanced grain growth that in turn results in increased absorption, modify thermal gradients, enhance compaction and increase thermal conductivity that all feedback on the net energy balance. The introduction of melting complicates things further by decreasing the number of ice-air boundaries which reduces scattering and enhances absorption of shortwave radiation (cf. Gardner & Sharp, 2010). If melting is sufficient to overcome capillary forces it will descend vertically within the snow/firn column redistributing large amounts of energy though latent heat release upon freezing or mass though encountering an impermeable surface and moving horizontally within the firn (cf. Coléou & Lesaffre, 1998; Marchenko et al., 2017). This complex interplay of surface processes creates non-linear responses to changes in surface forcing that require detailed modeling of the underlying physical processes.

Modern firn modeling draws heavily on the model physics implemented within seasonal snow models that have been developed for hydrology applications and avalanche forecasting. A few of the more widely used snow models include SnowPack (Bartelt & Lehning, 2002), CROCUS (Brun et al., 1989) and SnowModel (Liston and Elder, 2006). For a more comprehensive discussion of processes relevant for modeling of seasonal snow, readers should refer to the provided references and those that follow. Here we review those aspects relevant to modeling of perennial firn over ice sheets.

Early numerical modeling of firn was motivated by ice core research with an emphasis on understanding bore-hole temperature, ice age and pore close-off that is needed to determine gas age (e.g. Herron and Langway, 1980; Greuell & Oerlemans, 1989). Since, firn models have become critical to the estimation of the surface mass budget of the ice sheets (e.g. Pfeffer et al. 1991; Janssens & Huybrechts, 2000) as they are needed to model the vertical movement of meltwater within the snow and firn, and to determine if the meltwater refreezes in place or moves horizontally following the hydrologic gradient (Marsh & Woo, 1984; Pfeffer et al. 1990). Subsequent firn modeling efforts suggest that a warming climate will result in a steady decrease in the Greenland Ice Sheet's capacity to retain meltwater due to a reduction in firn pore space (van Angelen et al., 2013), a finding that has been supported by in situ observations (Vandecrux et al., 2019). More recent observations of extensive "firn aquifers" in Greenland that persists throughout the winter, when snow accumulation and melt rates are high (Forster et al., 2014), have proven the utility of firn modeling for understanding newly discovered phenomena (Steger et al., 2017).

https://doi.org/10.5194/egusphere-2022-674
Preprint. Discussion started: 16 August 2022

With the launch of the first satellite altimeters in the late-1970s it became possible, for the first time, to measure large-scale changes in ice sheet topography (Zwally et al., 1989). However, the interpretation of such changes were challenging due to unknown changes near-surface snow and firn density (Van Der Veen, 1993). The challenge is that changes in the near-surface density (i.e. changes in the firn air content: FAC) can cause changes in surface elevation without any corresponding changes in mass. By the late 1990s, numerical firn models were being used to estimate the uncertainties in the conversion of elevation change to mass change (Arthern & Wingham, 1998) and by the mid-2000s were being used to estimate the ice sheet wide changes in FAC for ice sheet wide estimation of mass change from satellite altimetry data (Zwally et al., 2005). Despite significant advances in firn modeling over the past decade and a half (e.g. Bougamont & Bamber, 2005; Ligtenberg et al., 2011), models still have significant deficits (Lundin et al., 2017; Vandecrux et al., 2020) and remain the largest source of uncertainty when inferring ice sheet mass change from satellite altimetry (Smith et al., 2019).

Here we present a new coupled surface energy balance and firn model, the Glacier Energy and Mass Balance model (GEMB, the "B" is silent) that has been integrated as a module into the Ice-sheet and Sea-level System Model (ISSM). Here we describe the state of GEMB as of Version 1.0. ISSM is an open-source software framework for modeling ice sheets, solid earth, and sea-level response that is developed at NASA's Jet Propulsion Laboratory (JPL) in conjunction with the University of California, Irvine and Dartmouth College (Larour et al., 2012). The DAKOTA software is embedded within the ISSM framework, facilitating uncertainty quantification and sensitivity studies (Larour et al., 2012a,b; Schlegel et al., 2013,2015; Schlegel and Larour, 2019). GEMB is responsible for the calculation of ice sheet and glacier surface-atmospheric energy and mass exchange and firn state within ISSM. It is a column model (no horizontal communication) of intermediate complexity that includes those processes deemed most relevant to glacier studies with the goal of retaining computational efficiency that can accommodate the very long (thousands of years) spin-ups necessary for initializing deep firn columns and for running sensitivity experiments to characterize model uncertainty on continental scales. GEMB is not coupled with a model of the atmosphere and instead runs offline, forced with climate reanalysis or climate model data. This approach allows flexibility in selection of forcing datasets at the expense of simulating surface-atmosphere feedbacks.

2. Model Description

GEMB is a vertical 1-D column model, i.e. no horizontal communication between model nodes, that simulates atmosphere-surface mass and energy exchanges and the internal evolution of snow, firn and ice. The model shares many characteristics with earlier published firn models that also simulate atmosphere-surface exchanges (e.g. Bassford, 2002; Bougamont & Bamber, 2005; Greuell & Konzelmann, 1994). The model is a finite-difference model with tens to hundreds of layers, the thickness of which are managed dynamically. It is forced at its surface with near-surface (2-10 m) estimates of precipitation, air temperature, wind speed, vapor pressure, surface pressure, and downwelling longwave and shortwave radiation fluxes and optional inputs of solar zenith angle, cloud optical thickness and bare ice albedo. At its bottom boundary, the model applies a constant thermal flux.

https://doi.org/10.5194/egusphere-2022-674
Preprint. Discussion started: 16 August 2022

Internally, the model simulates thermal diffusion, shortwave sub-surface penetration, meltwater retention, percolation and refreeze, effective snow grain size, dendricity, and sphericity, and compaction. The model does not yet account for changes in firn due to horizontal advection of divergence of the ice (Horlings et al., 2021). In this section we detail specific implementation of various processes, and their options, within the model.

2.1. Layer Initialization

GEMB is a finite difference model that simulates the snow-firn-ice as a number of discrete plane-parallel vertical layers, each with their own state parameters. The thickness (dz) of each vertical layer is initialized according to default or user supplied specification of the minimum and maximum thickness. The user can specify the maximum near-surface thickness (dz_{top}, default = 0.05 m), the depth of the near-surface (z_{top}, default = 10 m), the maximum column depth (z_{max}, default = 250 m) and a unitless scaling by depth parameter (β, default = 1.025). The thickness of each layer and the depth of the snow-firn-ice column is then determined as shown in Figure 1. The user can also specify a minimum near-surface thickness (dz_{min}) and a minimum column depth (z_{min}). If a layer thins to less than dz_{min} then it is combined with the layer directly below. If the total depth of the column is less than z_{min} then an additional ice layer is added to the bottom of the column.

2.2. Grain Growth

The model's master time step (i.e. the time step for all processes excluding the thermal model) is set by the timestep of the input data (typically on the order of hours). For all time steps, the first calculation of the GEMB model is done by the grain growth module. This module tracks and evolves the effective grain radius, dendricity, and sphericity of all model layers through time. These properties evolve according to published laboratory estimates for dendritic (Brun et al., 1992), non-dendritic (Marbouty, 1980), and wet snow metamorphism (Brun et al., 1989) that are dependent on mean layer temperature and density, and on gradients in temperature.

2.3. Shortwave flux

After the grain properties of all model layers are determined, GEMB runs the albedo module. GEMB provides five methods for calculating broadband surface albedo. The default albedo scheme is after Gardner and Sharp (2009), where albedo is calculated as a function of grain specific surface area ($\hat{S}$), concentration of light-absorbing carbon (c: optional), solar zenith angle (u': optional), and cloud optical thickness (τ: optional).

$$\alpha = \alpha_{\hat{S}} + d\alpha_c + d\alpha_{u'} + d\alpha_\tau$$

https://doi.org/10.5194/egusphere-2022-674
Preprint. Discussion started: 16 August 2022

Where $\alpha_{\hat{S}}$ is the pure snow albedo, $d\alpha_c$ is the change in albedo due to the presence of light-absorbing carbon, $d\alpha_u$, is the change in albedo due changes in the solar zenith angle, and $d\alpha_\tau$ is the change in albedo due to changes in the cloud optical thickness. Equations for each of the 4 components that sum to the net broadband albedo are provided in Equations 7 - 11 in Gardner and Sharp (2009).

Surface broadband albedo can also be calculated based on the effective grain radius (r_e), where broadband albedo is determined as a summation of the albedo within three spectral bands of solar irradiance (Brun et al., 1992, Lefebre et al., 2003). Effective grain radius can be related to specific surface area as:

$$r_e = \frac{3}{\rho_i \hat{S}}$$

Where ρ_i is the density of ice (910 kg m^{-3}).

Additionally, the surface albedo can be parameterized as a function of snow density and cloud amount according to Greuell & Konzelmann (1994) or as combination of exponential time decay and firn wetness following Bougamont & Bamber (2005).

The albedo of bare ice (defined by a density threshold, default of 820 kg m^{-3}) can be set as a constant everywhere or spatially varying when provided on the model grid (e.g. as derived from MODIS). Alternatively, the ice albedo and shallow snow-covered (<10 cm in depth) ice albedo can be parameterized as a function of model-estimated accumulation of surface meltwater following Alexander et al. (2014).

When shortwave radiation reaches the glacier surface it is scattered and absorbed. The fraction of energy that is scattered then reflected back to the atmosphere is dictated by the modeled broadband albedo. The remainder of the energy is absorbed within the snow, firn and ice. By default, GEMB will allocate all absorbed energy to the top model layer (subsurface absorption turned off) but also allows for the absorbed radiation to be distributed within near-surface (i.e. across multiple near surface layers: subsurface absorption turned on). When the subsurface absorption is turned on, the amount of shortwave radiation absorbed within each model layer is dependent on which albedo scheme is used. If the albedo scheme is based on effective grain radius, then the subsurface absorption is calculated in three spectral bands, dependent on effective grain radius as described by Brun et al. (1992). In all other cases, the subsurface albedo is treated as a function of each layer's snow density (Bassford, 2002; Bassford et al., 2006). In this case a specified fraction of the shortwave radiation (approximately 36%) is absorbed by the surface layer (Greuell and Konzelmann, 1994), with the rest of the energy being absorbed at depth with consideration to Beer's law (Bassford, 2002).

https://doi.org/10.5194/egusphere-2022-674
Preprint. Discussion started: 16 August 2022

2.4. Thermodynamics

The thermodynamics module is responsible for determining the temperature of the snow, firn, and ice. Temperature evolves according to thermal diffusion, in response to radiative, sensible and latent heat fluxes. The thermal conductivity of snow and ice is calculated according to Sturm et al. 1997 (default) or Calonne et al., 2011. The thermal diffusion calculation is executed at a much finer timestep than the master timestep, 10s of seconds versus hours. The finer time step is required to satisfy the Courant–Friedrichs–Lewy condition, a necessary condition to ensure numeric stability of the thermal solution (Courant et al., 1928). The small timestep for the thermal diffusion makes this module, by far, the most computationally expensive component of GEMB. The thermal module is looped within each GEMB timestep and therefore the thermal time step must divide evenly into the model's master time step. The thermal conductivity is calculated as a function of density, for densities < 910 kg m^{-3}, and as a function of temperature, for >= 910 kg m^{-3}. Thermal diffusion coefficients are then calculated using a discretization scheme which truncates the Taylor-Series expansion after the 3rd term (Patankar 1980, Ch. 3&4). The minimum acceptable thermal timestep is calculated, dependent upon the thermal conductivity, and then divided by a scaling-factor to achieve numerical stability. Within every timestep, the thermal module calculates the diffusion of temperature within the snow, firn and ice.

At each thermal diffusion timestep the module determines the radiative and turbulent fluxes (Patterson, 1994; Murphy and Koop, 2005), rates of evaporation/condensation, and the new temperature profile throughout the model depth. Layer temperatures are allowed to artificially exceed the melting point of ice (273.15 K), the thermal energy above which is later converted to melt by the melt module. That said, the surface temperature used for computing the outgoing longwave energy and turbulent heat flux is taken as the lesser of the temperature of the top model layer or 273.15 K. The snow/ice is assumed to be a black body (default emissivity = 0.97) with the incoming longwave radiation absorbed within the top layer and outgoing longwave radiation calculated using the Stefan-Boltzmann constant (5.67E-8 W m^{-2} K^{-4}). Calculation of turbulent fluxes is defined in the next subsection. At the end of the thermodynamics module, any mass lost/added by evaporation/condensation is removed/added to the top layer.

2.5. Turbulent Flux

Turbulent fluxes and evaporation/sublimation/condensation are computed within the thermodynamics module using the bulk method. The bulk transfer coefficient is calculated based on momentum roughness length and the height at which air temperature and wind speed inputs are provided. The momentum roughness length is set to 0.12 mm for dry snow, 1.3 mm for wet snow and 3.2 mm for ice, after Bougamont et al. (2005), and the humidity and temperature roughness lengths are set to 10% of these values (Foken, 2008). Within each thermodynamics time step, the model calculates the bulk Richardson number (*Ri*) and determines the Monin-Obukhov stability parameters for weighting the sensible and latent heat flux (Ohmura, 1982). In stable conditions (i.e., *Ri*>0), the stability weighting parameters are determined after Beljaars and Holtslag (1991) (Ding et al., 2020), and in unstable conditions (i.e., *Ri* <= 0), the stability weighting parameters are determined after Högström (1996) as in Sjöblom, 2014. To determine the latent heat flux, the model calculates the surface vapor pressure for

https://doi.org/10.5194/egusphere-2022-674
Preprint. Discussion started: 16 August 2022

liquid water or ice (Murphy and Koop, 2005), depending on whether the surface is wet (Murray, 1967) or dry (Bolton, 1980), respectively. The sensible and latent heat are then determined as a function of the bulk transfer coefficient, Monin-Obukhov stability parameters, the surface temperature (lesser of the temperature of the top model layer or 273.15 K), near-surface air temperature, near-surface wind speed, near-surface vapor pressure, and the air pressure at the surface. Longwave emissivity can be set by the user, with a default of 0.97. Mass transfer due to evaporation/sublimation/condensation is based on the latent heat flux along with the latent heat of evaporation/condensation (gas <-> liquid) or the latent heat of sublimation (solid <-> gas).

2.6. Accumulation

The GEMB accumulation module is responsible for the addition of mass due to precipitation and related modification of uppermost layer properties (i.e. density, temperature, dendricity, sphericity, and grain radius). When precipitation occurs and the air temperature is below the melting point, the model accumulates precipitation as snow at the surface. The density of newly fallen snow can be set to a default value, i.e., 350 kg/m^3 (Weinhart et al., 2020) for Antarctica or 315 kg/m^3 (Fausto et al., 2018) for Greenland, or it can be parameterized as a function of the annual temperature, accumulation, surface pressure and wind speed according to Kaspers et al. (2004) or as a function of annual temperature according to Kuipers Munneke et al. (2015). Initial dendricity is by default set to 1, and initial sphericity is set to 0.5. For Greenland, we consider wind effects on the snow's initial dendricity and sphericity following Guyomarc'h and Merindol (1998) as in Vionnet et al. (2012). In the case where the air temperature is at or exceeds the melting point, precipitation is treated as rain, and liquid water is added to the uppermost model layer. When this occurs, the surface layer properties, specifically temperature and density, are updated to account for the addition of mass as ice and the release of latent heat. Any thermal energy exceeding the melting point of ice will be converted back to liquid water by the melt module and allowed to percolate.

If the newly accumulated mass exceeds the minimum allowable top-layer layer thickness (dz_{min}), the accumulation is added as a new surface layer. Otherwise the snow is added to the existing surface layer, and the surface properties are adjusted to accommodate the accumulation by averaging properties, weighting by mass, with the exception of dendricity and sphericity, which take the value of the newly accumulated snow. New snow that is accumulated is assumed to have the same temperature as the near-surface air temperature.

2.7. Melt

After new mass is accumulated within the top layer(s), the melt module is run. This module is responsible for calculating how much melt will occur throughout the model column, how much of the melt will percolate into layers below, how much of this melt will refreeze, how much of the melt will runoff, and how the temperature of each layer will evolve accordingly. GEMB uses a bucket scheme (cf. Steger et al., 2017) to model the vertical movement of meltwater within the firn. The first step of

https://doi.org/10.5194/egusphere-2022-674
Preprint. Discussion started: 16 August 2022

this scheme is to determine how much of the current pore water in the firn column can be refrozen without heating the firn layer above the freezing point of ice. If this water does exist, it is refrozen locally, and the model layers' physical and thermal properties are updated in response to this process. The next step is to determine where melt will occur. Beginning with the surface layer, the module determines if the local thermal energy is capable of melting any of the ice within the layer, and if it is, this portion of the layer is melted and any excess thermal energy or melt water that cannot be accommodated in the pore space locally is redistributed to the layer below. As the meltwater is distributed to lower layers, it may reach a layer of impermeability (density of pore hole close-off, ~830 kg/m^3), and at this point, that meltwater exits the system and is considered runoff. If the layer below is permeable and the pore space can accommodate incoming meltwater, the water that can be retained within that layer is combined with any existing liquid water. If any portion of the incoming meltwater cannot be accommodated within the layer, it percolates (instantaneously) to the layer below. Water that remains is refrozen locally, within each layer, but only until the local temperature reaches the freezing point (273.15 K). Meltwater that reaches the deepest layer of the column exits the system and is considered by the model to be runoff. Runoff from all layers of a column are summed to determine the total amount of melt that runs off (i.e. exits the model domain).

2.8. Layer Management

After the melt/refreeze/runoff calculations are complete, the melt module ensures that the thickness of any single layer does not exceed thresholds set for the minimum and maximum allowable layer thickness. This is done through the merging or splitting of model layers and associated changes in layer properties. Specifically, this module ensures that layering within the column adheres to: the user-defined minimum thickness for a layer (dz_{min}); the user-defined maximum change in depth between adjacent layers (β, default = 1.025 or 2.5% change between layers); and the user-defined maximum (z_{max}) and minimum (z_{min}) depths of the total column (with default values of 250 m and 130 m, respectively). Before completion, the melt module checks for the conservation of mass and energy, and throws an error if these values are not conserved. If the maximum column depth is exceeded, mass is removed from the bottom layer. If the depth of the model falls below the minimum allowable depth, then ice is added to the bottom layer of the model with identical properties as possessed by the bottom layer. All additions and subtractions of mass are cataloged and accounted for in final mass change estimates.

2.9. Densification

After the merging/splitting of model layers, GEMB runs the densification module. This module calculates how much the snow and firn layers compact (increases in density) over the master time step. The densification module offers seven different approaches for computing densification rate factors: Herron and Langway (1980); Arthern et al. (2010) (semi-empirical model and physical model); Li and Zwally (2004); and Helsen et al. (2008). Regardless of the approach used, grain sliding dominated compaction (density <= 550 kg/m^3) is treated independently from sintering and bubble compression dominated compaction (>550 kg/m^3). Densification rate parameters for layers above/below the 550

https://doi.org/10.5194/egusphere-2022-674
Preprint. Discussion started: 16 August 2022

kg/m^3 density threshold, are calculated by this module. These parameters are then used to calculate densification rates after Herron and Langway (1980), and a new density profile for the column is determined.

In addition to the densification models, GEMB implements a calibration of the Arthern et al. (2010) model that was developed by Ligtenberg et al. (2011) for the Antarctic and applied by Kuipers Munneke et al. (2015) to Greenland. Using the semi-empirical model for dry snow densification, as described by Arthern et al. (2010) in Appendix B, the *c0* and *c1* rate parameters are scaled by model-to-observed calibration values ($M0_{550}$ for density <= 550 kg/m^3 and $M0_{830}$ for densities between 550 kg/m^3 and 830 kg/m^3) that are trained by a comparison between firn core density profiles and modeled density profiles with respect to a climatological mean accumulation rate (C):

$$MO_{550/830} = b_{550/830} + m_{550/830} * ln(C)$$

Where 550/830 indicates coefficients for modeling of densities <= 550 kg m^{-3} and between 550 kg m^{-3} and 830 kg m^{-3}, respectively.

3. Study specific model setup

3.1. Parameterization selection

GEMB v1.0 has many options for various model parameterizations. For this study we use a simplified version of the Gardner and Sharp (2009) albedo scheme in which albedo is modeled solely as a function of snow/ice grain specific surface area ($\hat{S}$). Sub-surface shortwave penetration is turned off. Bare ice and shallow snow-covered ice albedo (areas with a surface density > 820 kg/m^3) are spatially varying and derived from the MODIS MCD43C3 16-day black-sky albedo product (Schaaf et al, 2015). Here, we determine the bare-ice albedo by taking all summer (J,J,A) MCD43C3 16-day black-sky albedo values and calculating the lowest 10th percentile of measured albedos for every grid location. Bare ice albedos are not allowed to be less than 0.4. Albedos are then smoothed to a 0.25 degree (~32 km) resolution then bilinearly interpolated onto the GEMB model grid. The full list of selected model parameters used for this study are provided in Table 1.

3.2. Model grid

GEMB has no horizontal communication and thus easily supports non-uniform grid spacing for computational efficiency, i.e. the model does not need to be run at the same spatial resolution as the climate forcing. This allows the model to use a coarser resolution grid for areas with small spatial gradients in surface forcing (e.g. flat ice sheet interiors) and to use a refined grid in areas of steep spatial gradients (e.g. areas of complex topography or near ice-ocean boundaries). For the simulations presented here, we use a Greenland grid with 10990 nodes with node pacing ranging from 0.7 km along the coast to 21.1 km in the interior. For the Antarctic we use a grid with 50390 nodes with node spacing ranging from 3.7 km along the periphery to 33.3 km in the interior. Both grids are shown in Figure 2.

https://doi.org/10.5194/egusphere-2022-674
Preprint. Discussion started: 16 August 2022

3.3. Atmospheric Forcing

For this study we force GEMB with climate data from the regional atmospheric climate model RACMO2.3p2 for the Antarctic (van Wessem et al., 2018) and RACMO2.3 for Greenland (Noël et al., 2015). Atmospheric fields of 10-m wind speed and 2-m temperature, surface pressure, incoming long- and short-wave radiation, vapor pressure, and precipitation are supplied at 3 hour resolution. The Antarctic product is provided at 27 km horizontal resolution for years 1979 through 2014 and Greenland data at 11 km resolution for years 1979 through 2014.

3.4. Firn model calibration

GEMB is run with the uncalibrated semi-empirical Arthern et al. (2010) firn model and is forced with a repeated cycle of historical climatology until a steady-state density profile is reached, e.g., about 5000 years for Greenland and 6000 years for Antarctica. The depths of the modeled density horizons are extracted at the end of this spin-up procedure, from the model grid elements which are closest in location to the firn cores used for calibration (Figure 3). Here we use 64 shallow firn cores and 15 deep firn cores for calibration of Greenland firn and 117 shallow and 29 deep firn cores for calibration of Antarctic firn (Montgomery et al., 2018; Smith et al., 2020; *Medley et al., 2020*). Firn cores are classified as shallow if they reach the 550 kg/m^3 density horizon and deep if they extend to the 830 kg/ m^3 density horizon.

For these firn core locations, MO_{550} and MO_{830} are plotted independently as functions of the natural log of C (Figure 4). A line is then fit through the points for each, representing the linear expression of how the model-to-observed depths vary as a function of C at each horizon. Next, the model steady-state spin-up is repeated, but this time multiplying the rate coefficients of *c0* and *c1*, of the semi-empirical model of Arthern et al. (2010), by MO_{550} and MO_{830}, respectively. Following Ligtenberg et al. (2011), MO_{550} and MO_{830} are allowed a minimum value of 0.25. Derived calibration coefficients $b_{550/830}$ and $m_{550/830}$ are provided in Table 1.

The new steady-state model density profiles are then verified against the calibration subset of firn cores as well as an additional withheld subset.

4. Comparison to current state-of-the-art

4.1. Surface Mass Balance

Here we compare GEMB v1.0, surface mass balance components to those computed within the RACMO surface model: RACMO2.3p2 for the Antarctic (van Wessem et al., 2018) and RACMO2.3 for Greenland (Noël et al., 2015). Since both GEMB and RACMO surfaces are forced with the same atmospheric data (RACMO), differences between modeled components can be directly attributed to differences in how surface processes are treated (e.g. albedo, roughness lengths, thermal diffusion, etc.).

https://doi.org/10.5194/egusphere-2022-674
Preprint. Discussion started: 16 August 2022

We also note that the RACMO surface model accounts for feedbacks between the atmosphere and the surface, while GEMB does not.

Mean spatial patterns of surface mass balance (i.e. accumulation minus ablation) are shown for both ice sheets and both models in Figure 5 and Figure 7. The SMB patterns for the Antarctic ice sheet are driven largely by snowfall and sublimation, with little contribution from meltwater runoff. In Greenland, snowfall and runoff dominate. This largely explains the much closer agreement between models in the Antarctic vs. Greenland.

In Greenland the largest differences between models are concentrated to areas of high melt and low elevation that comprise the ice sheet periphery. In general, GEMB produces more negative surface mass balance in areas of maximum melt and slightly less negative surface mass balance near the equilibrium altitude. The more negative surface mass balance at lower elevations is most likely caused by a lower "bare ice" albedo in GEMB than in RACMO. Higher surface mass balance near the equilibrium line altitude is likely due to lower rates of fresh snow melt. For the Antarctic, differences can largely be summarized as GEMB having higher rates of melt and runoff along the ice sheet periphery and lower rates of sublimation in areas conducive to katabatic winds (Parish & Bromwich, 1987). GEMB's higher rates of melt are most likely driven by lower surface albedo. Lower rates of sublimation can be attributed to the fact that GEMB does not yet (as of v1.0) include a model for snowdrift sublimation while RACMO does (Lenaerts et al., 2010).

Looking at Greenland (Figure 8) and Antarctic (Figure 9) monthly (a) and cumulative (b) time series of surface mass balance components we find very close agreement between GEMB and RACMO. Agreement is so close that several RACMO variables are not visible in the monthly time series (Figure 8a & Figure 9a) as they are overlain by near-identical GEMB output. The most notable difference is higher rates of melt for RACMO simulations in Greenland that are largely compensated for by increased meltwater retention within the firn. In the Antarctic lower rates of sublimation in the Antarctic and higher rates of meltwater runoff lead to a slightly more positive surface mass balance trend.

4.2. Firn Air Content

Next, we compare firn properties as modeled by GEMB v1.0 to those modeled by the Institute for Marine and Atmospheric Research Utrecht Firn Densification Model (IMAU-FDM: Ligtenberg et al. 2011) run for Greenland (Ligtenberg et al. 2018) and the Antarctic (Ligtenberg et al., 2011) forced with the same RACMO data as used by the GEMB simulations (see Study specific model setup and Table 1). Like GEMB, IMAU-FDM is an uncoupled firn model (i.e. not coupled with the atmospheric model). IMAU-FDM represents the state-of-the-art in ice sheet firn modeling. We next look at the spatial patterns of total Firn Air Content (FAC), the depth of air in meters per unit area. For Greenland, GEMB tends to generate lower FAC in the West and South-East percolation zones along the ice sheet margins and a slightly higher FAC in the North East (Figure 6). This is counterintuitive as GEMB is shown to produce less melt than RACMO in areas where RACMO has a higher FAC, we would expect the opposite to be true. This difference is likely the result of a slightly more aggressive compaction

https://doi.org/10.5194/egusphere-2022-674
Preprint. Discussion started: 16 August 2022

calibration scaling coefficient used by GEMB (Table 1: $b_{550/830}$ = 1.27/2.00, $m_{550/830}$ = -0.12/-0.25*)* relative to those used by FDM ($b_{550/830}$ = 1.04/1.73, $m_{550/830}$ = -0.09/-0.20).

In the Antarctic there is generally better agreement between models and scaling coefficients of $b_{550/830}$ = 1.64/2.00, $m_{550/830}$ = -0.17/-0.24 for GEMB and $b_{550/830}$ = 1.44/2.37, $m_{550/830}$ = -0.15/-0.29 for FDM (Kuipers Munneke et al., 2015). Differences between GEMB and FDM can be characterized as GEMB having lower FAC at low elevations and slightly higher FAC at higher elevations (Figure 7). This pattern can be attributed to GEMB having warmer surface temperatures (higher melt) at lower elevations and smaller b_{830} scaling coefficient that will impact total FAC most in areas with deep firn (i.e. the Antarctic Plateau).

Looking at the temporal evolution in FAC for both Greenland (Figure 8) and Antarctica (Figure 9) it can be seen that seasonal fluctuations and inter-annual variations are in very close agreement for both ice sheets but deviations in long-term trends are apparent. For Greenland (Figure 8) GEMB has virtually no trend in FAC between 1979 and 2005, becoming more negative thereafter coincident with increases in summer melt. FDM FAC trends positive 1979 and 2005 after which the trend becomes negative, closely matching the rate of FAC loss simulated by GEMB. Differences in FAC trend between 1979 and 2005 can be attributed to differences in model spin-up that are known to be a major source of uncertainty in FAC trends (Kuipers Munneke et al., 2015). GEMB uses the 1979-1988 climatology repeated for 5000 year for its spin-up while FDM uses the 1960–1979 climatology repeated as many times as required until the mean annual accumulation rate multiplied by the spin-up length equals the thickness of the firn layer (from the surface to the depth at which the ice density is reached: Kuipers Munneke et al., 2015). Because GEMB is initialized to the repeated 1979-1988 climatology, there should be little trend in FAC over this period. GEMB was initialized to the 1979-1988 climatology as the 1960-1979 period was not included with the provided RACMO forcing and climate reanalysis perform considerably better after the introduction of satellite data in 1978, this is especially true over the poles where in situ observations are sparse (Tennant, 2004). This difference in prescribed spin-up climatology is the most likely cause of the observed differences in FAC trend between 1979 and 2005. When the 1979-2005 FAC trend is removed from both products (not shown), the FAC time series are nearly identical until 2004 after which GEMB estimates ~0.5 m of FAC loss and FDM estimates ~1.0 m of FAC loss between 2004 and 2015. Some of the difference in trend can be attributed to FDM having higher rates of melt along the ELA during this period of time (Figure 5).

Changes in FAC for the Antarctic (Figure 9) are nearly identical between models with a notable divergence beginning in 2008, after which GEMB FAC trends slightly positive and FDM FAC trends slightly negative. Spatial patterns of FAC trends for the period pre- and post-2008 (Figure 10) show much larger rates of FAC for the 2008-2015 period with FDM tending to have the same sign but larger trends than GEMB. For the post 2008 period, GEMB FAC gains outcompete losses resulting in a slight positive trend in FAC over this period that is not seen in FDM.

Despite a desire to identify which model is closer to the truth, we do not yet have an objective way to determine that. Likely the most definitive analysis will be to compare FAC corrected altimetry (e.g.

https://doi.org/10.5194/egusphere-2022-674
Preprint. Discussion started: 16 August 2022

ICESat/2) estimates of ice sheet mass change to mass changes derived from satellite gravimetry (i.e. GRACE/FO) data, but that is beyond the scope of this study.

5. Model sensitivity to vertical resolution

Firn and surface mass balance models are highly sensitive to the chosen setup and empirical parameterizations (Bougamont et al., 2007; Kuipers Munneke et al., 2015). Major sources of uncertainty include parameterizations of albedo, snow grain growth, surface roughness, densification and its calibration (Stevens et al., 2020), and thermal conductivity. These uncertainties become exacerbated with the introduction of liquid water into the firn column (Vandecrux et al., 2020). Model setup can also introduce large sources of uncertainty and error. Four particularly important decisions are the choice of spin-up climatology (Kuipers Munneke et al., 2015), the length of time the spin-up is run (needs to reach equilibrium to prevent model drift), and the vertical resolution of the model. Most of these sensitivities have been explored extensively and we direct the reader to previous publications that explore these topics in detail (e.g. Bougamont et al., 2007; Kuipers Munneke et al., 2015; Vandecrux et al., 2020; Stevens et al., 2020; Lundin et al., 2017).

One model sensitivity that we have not seen covered elsewhere is the sensitivity of the model to the vertical resolution of the firn column. The vertical resolution can have a large impact on melt rates and surface temperatures. This is because all of the energy and mass transfer between the atmosphere and the surface is often allocated to the model's uppermost layer in the firn column. A thicker layer will tend to dampen fluctuations in thermal energy relative to a thinner layer. Since snow grain growth, snow/ice melt, and compaction have non-linear relations to temperature, model results will diverge for differing vertical resolutions. This is most true for the near-surface layers as thermal gradients are attenuated with depth.

To demonstrate model sensitivity to vertical resolution we run GEMB v1.0 for Greenland using the same model setup (Table 1) but for four different dz_{top} [2 cm, 5 cm, 10 cm, 20 cm] and dz_{min} [1 cm, 2.5 cm, 5 cm, 10 cm] pairs. Results of the simulations are shown in Figure 11. Increasing the size of the top layers results in a progressive reduction in melt as diurnal peak temperatures are muted and vertical gradients in temperature are reduced, in turn reducing grain metamorphism and surface darkening. Increasing the size of the top layers also results in stronger thermal gradients between the atmosphere and the surface that drive larger (both positive and negative) surface latent and sensible heat and mass fluxes. This has more impact in summer when diurnal fluctuations are larger than during polar night when diurnal changes in temperature are small or non-existent. The net effect of increasing the surface layer thickness is slightly lower evaporation/sublimation losses.

6. Comparison of modeled and observed near-surface temperatures

To demonstrate the model's skill at simulating near-surface temperature, we compare GEMB v1.0 model output to an observational dataset of near-surface firn temperature that was collected at the

https://doi.org/10.5194/egusphere-2022-674
Preprint. Discussion started: 16 August 2022

Summit Station, Greenland (Miller et al., 2017). Here, subsurface temperatures are measured using thermistors buried within the snowpack every 20 cm, from July 2013 to June 2014. We compare these observations against results produced by GEMB v1.0 forced with RACMO output (see Table 1), rerun to output concurrent daily model solutions for the location of the observations (72.580° N, 38.459° W). By default, GEMB's thermal conductivity is calculated as a function of snow density, after Sturm et al., 1997. To investigate model sensitivity to thermal conductivity, we also run the same simulation using the density-dependent thermal conductivity relation suggested by Calonne et al., 2011. As demonstrated by Calonne et al., 2011, their solution gives a higher thermal conductivity for an equivalent density, which sits just inside of the upper bounds of the 95% confidence interval reported by Sturm et al., 1997. Here we compare results between the two GEMB simulations and the observations. For simplicity, all results are plotted with respect to the modeled or observed surface. Note that since the first thermal probe was placed at a depth of 20 cm below the surface, observational values between the snow surface and 20 cm depth are extrapolations.

Figure 12 a, c and e show the thermal profiles to a depth of 2m for observed, GEMB-Sturm and GEMB-Calonne temperatures, respectively. Figure 12 b shows the observed radiative fluxes and Figure 12 d and f show the difference between modeled and observed snow temperature profiles. Overall, there is very good agreement between the modeled and observed thermal profiles with differences resulting from errors in atmospheric forcing, errors in observations, and biases attributed to errors in model parameterizations. Both model simulations produce mean temperatures between 0.2 and 2 meters depth that are ~0.8 K warmer than the observations, with the Sturm parameterization of thermal conductivity producing slightly better agreement (0.77 K) than the Calonne parameterization (0.79 K). Looking at bias and root-mean-square error as a function of depth, it can be seen (Figure 13) that the Sturm parameterization produces slightly better agreement to the observations in the top 0.5 meters of the snow pack while the Calonne parameterization produces significantly better fit for depths below 0.8 meters. From this single location comparison, the Calonne parameterization outperforms the Sturm parametrization. Drawing any more definitive conclusions is challenging given other sources of disagreement such as atmospheric forcing and density structure.

7. Summary and Conclusions

This paper provides the first description of version 1.0 of the open-source Glacier Energy and Mass Balance model that has been integrated as a module into the Ice-sheet and Sea-level System Model (ISSM). The model is one-way coupled with the atmosphere which allows the model to be run off-line with a diversity of climate forcing but neglects feedback to the atmosphere. GEMB is written in C++ which produces efficient compiled machine code for fast execution. GEMB provides numerous parameterization choices for various key processes (e.g. albedo, subsurface shortwave absorption, and compaction), making it well suited for uncertainty quantification and model exploration.

To evaluate output from GEMB we compare it to the model output from the Institute for Marine and Atmospheric Research Utrecht Firn Densification Model (IMAU-FDM: Ligtenberg et al. 2011) for both

https://doi.org/10.5194/egusphere-2022-674
Preprint. Discussion started: 16 August 2022

Greenland (Ligtenberg et al. 2018) and the Antarctic (Ligtenberg et al., 2011). Models are forced with the same RACMO climate data (see Study specific model setup: Table 1) and are independently calibrated to ice core density profiles. By forcing GEMB with the same climate data as IMAU-FDM we are able to attribute differences in model output to differences in model parameterizations and setup.

Overall, we find good agreement between models for both ice sheets with a few notable differences. For Greenland GEMB produces considerably less melt than IMAU-FDM but nearly as much runoff. This is because, relative to IMAU-FDM, GEMB tends to generate more low elevation melt that runs off and less high elevation melt that refreezes within the firn. These differences are most likely due to inter-model differences in the bare ice albedo and fresh snow melt. GEMB and IMAU-FDM produce considerably different trends in FAC that are the result of differing climatologies used for model spin-up. GEMB used the 1979-1988 climatology repeated for 5000 years while IMAU-FDM used the 1960-1979 climatology. This results in GEMB having little trend in FAC prior to the onset of increased melting in 2005. In contrast, IMAU-FDM has a positive FAC trend from 1979-2005 and a negative trend thereafter. These differences can have a large impact on volume-to-mass conversions used to generate glacier mass change estimates from satellite altimetry. For the Antarctic, GEMB and IMAU-FDM are nearly identical with GEMB having slightly lower rates of sublimation and slightly higher rates of meltwater runoff that lead to a slightly more positive surface mass balance trend than found in IMAU-FDM. Changes in FAC for the Antarctic are nearly identical between models with a notable divergence beginning in 2008, after which GEMB FAC trends slightly positive and FDM FAC trends slightly negative.

To demonstrate the impact of model setup we explore the impact of the model's vertical resolution on the results. We show that increasing the model's vertical resolution decreases melt and increases surface latent and sensible heat fluxes due to stronger thermal gradients between the surface and the atmosphere. Lastly, we compare modeled near-surface thermal profiles, calculated using two different density-thermal conductivity relations, to in situ observations collected at Summit Station, Greenland. Our comparison shows good agreement between modeled and observed temperatures, with slightly improved agreement using the Calonne versus the Sturm thermal conductivity parameterization.

Our analysis shows that the Glacier Energy and Mass Balance (GEMB) model performs as expected and produces results that are comparable to an existing state-of-the-art firn model (IMAU-FDM). However, there are notable differences in output between the models but it is difficult to judge if one model outperforms the other as there is insufficient observational data with sufficient accuracy to distinguish between models. Future studies that compare altimetry derived mass changes, with those derived from satellite gravimetry should help to distinguish between models.

Future work will focus on developing atmospheric and firn downscaling routines that will allow GEMB to produce higher resolution output when forced with medium resolution (30-100 km) climate reanalysis or coarse resolution (200-500 km) climate model output.

Code availability:

https://doi.org/10.5194/egusphere-2022-674
Preprint. Discussion started: 16 August 2022

GEMB can be downloaded as part of Ice-sheet and Sea-level System Model (ISSM: https://issm.jpl.nasa.gov/). An unmaintained MATLAB version of the model is also available (Gardner, A. S., 2022). It is recommended to use the well maintained ISSM version of GEMB.

Data availability:
All GEMB and RACMO/FDM model output used to generate Figures 1 through 13 can be found in Schlegel, N-J. et al. (2022).

Author contribution:
A.G. wrote the model, co-wrote the paper, and made the figures. N.S. ran all of the experiments and co-wrote the paper. E.L. translated the original model from Matlab into C++ and integrated it into ISSM.

Competing interests:
The authors declare that they have no competing interests.

Acknowledgements:
We thank Brooke Medley for sharing the firn core data. We thank Brice Noël, J.M. van Wessem, Stefan Ligtenberg, Michiel van den Broeke for sharing the RACMO climate forcing and IMAU-FDM results. We thank Nathaniel Miller for directing us to the Greenland temperature profile observations and we thank Martin Sharp for helping motivate early work on the model. The authors were supported by the NASA Cryospheric Sciences, ICESat-2, MEaSUREs, and the NASA Sea Level Change Team programs. We gratefully acknowledge computational resources and support from the NASA Advanced Supercomputing Division. The research was conducted at the Jet Propulsion Laboratory, California Institute of Technology, under contract with the National Aeronautics and Space Administration.

References

Alexander, P. M., Tedesco, M., Fettweis, X., van de Wal, R. S. W., Smeets, C. J. P. P., and van den Broeke, M. R., 2014: Assessing spatio-temporal variability and trends in modelled and measured Greenland Ice Sheet albedo (2000–2013), The Cryosphere, 8, 2293–2312, https://doi.org/10.5194/tc-8-2293-2014.

Alley, R. B. (1987). Firn densification by grain-boundary sliding: a first model. Le Journal de Physique Colloques, 48(C1), C1-249.

Arthern, R. J., Vaughan, D.G., Rankin, A.M., Mulvaney, R, and Thomas, E.R., 2010: In situ measurements of Antarctic snow compaction compared with predictions of models, J. Geophys. Res., 115, F03011, doi:10.1029/2009JF001306.

Arthern, R. J., & Wingham, D. J. (1998). The Natural Fluctuations of Firn Densification and Their Effect on the Geodetic Determination of Ice Sheet Mass Balance. Climatic Change, 40(3), 605–624. https://doi.org/10.1023/A:1005320713306

https://doi.org/10.5194/egusphere-2022-674
Preprint. Discussion started: 16 August 2022

Bartelt, P., & Lehning, M. (2002). A physical SNOWPACK model for the Swiss avalanche warning Part I: Numerical model. Cold Regions Science and Technology, 35(3), 123–145. file:///E:/Work_Computer/Articles/Articles/Bartelt, 2002. Cold Regions Sci %26 Tech. v35.pdf

Bassford, R. P., 2002: Geophysical and numerical modelling investigations of the ice caps in Severnaya Zemlya. Ph.D. thesis, University of Bristol, England.

Bassford, R. P., M. J. Siegert, J. A. Dowdeswell, J. Oerlemans, A. F. Glazovsky & Y. Y. Macheret (2006) Quantifying the Mass Balance of Ice Caps on Severnaya Zemlya, Russian High Arctic. I: Climate and Mass Balance of the Vavilov Ice Cap, Arctic, Antarctic, and Alpine Research, 38:1, 1-12, DOI: 10.1657/1523-0430(2006)038[0001:QTMBOI]2.0.CO;2

Beljaars, A. C. M., & Holtslag, A. A. M. (1991). Flux parameterization over land surfaces for atmospheric models. Journal of Applied Meteorology, 30(3), 327–341.

Bolton, D. (1980). The computation of equivalent potential temperature. Monthly Weather Review, 108, 1046–1953.

Bougamont, M., & Bamber, J. L. (2005). A surface mass balance model for the Greenland Ice Sheet. Journal of Geophysical Research-Earth Surface, 110(F4), doi:10.1029/2005JF000348.

Bougamont, M., Bamber, J. L., Ridley, J. K., Gladstone, R. M., Greuell, W., Hanna, E., Payne, A. J., & Rutt, I. (2007). Impact of model physics on estimating the surface mass balance of the Greenland Ice Sheet. Geophysical Research Letters, 34(17), doi:10.1029/2007GL030700. http://internal-pdf//Bougamont, 2007. GRL. v34-1931089158/Bougamont, 2007. GRL. v34.pdf

Brun, E., (1989). Investigation on wet-snow metamorphism in respect of liquid-water content. Annals of Glaciology, 13, 22-26.

Brun, E., P. David, M. Sudul, and G. Brunot, (1992). A numerical model to simulate snow-cover stratigraphy for operational avalanche forecasting. Journal of Glaciology, 38, 13-22.

Brun, E., Martin, E., Simon, V., Gendre, C., & Coleou, C. (1989). An energy and mass model of snow cover suitable for operational avalanche forecasting. Journal of Glaciology, 35(121), 333–342. file:///E:/Work_Computer/Articles/Articles/Brun, 1989. J Glaciology. v35.pdf

Calonne, N., Milliancourt, L., Burr, A., Philip, A., Martin, C. L., Flin, F., & Geindreau, C. (2019). Thermal Conductivity of Snow, Firn, and Porous Ice From 3-D Image-Based Computations. Geophysical Research Letters, 46(22), 13079–13089. https://doi.org/https://doi.org/10.1029/2019GL085228

Calonne, N., Flin, F., Morin, S., Lesaffre, B., du Roscoat, S. Rolland, and Geindreau, C. (2011), Numerical and experimental investigations of the effective thermal conductivity of snow, Geophys. Res. Lett., 38, L23501, doi:10.1029/2011GL049234.

Colbeck, S. C. (1982). An overview of seasonal snow metamorphism. Reviews of Geophysics and Space Physics, 20(1), 45–61. file:///E:/Work_Computer/Articles/Articles/Colbeck, 1982. Reviews of Geophysics and Space Physics. v20.pdf

https://doi.org/10.5194/egusphere-2022-674
Preprint. Discussion started: 16 August 2022

Coléou, C., & Lesaffre, B. (1998). Irreducible water saturation in snow: experimental results in a cold laboratory. Annals of Glaciology, 26, 64–68. https://doi.org/DOI: 10.3189/1998AoG26-1-64-68

Copernicus Climate Change Service (C3S): ERA5: Fifth generation of ECMWF atmospheric reanalyses of the global climate . Copernicus Climate Change Service Climate Data Store (CDS), date of access: Jan 25, 2019. https://cds.climate.copernicus.eu/cdsapp#!/home, 2017

Courant, R., Friedrichs, K., & Lewy, H. (1928). Über die partiellen Differenzengleichungen der mathematischen Physik. Mathematische Annalen, 100(1), 32–74.

Ding, M., Yang, D., van den Broeke, M., Allison, I., Xiao, C., Qin, D., & Huai, B. (2020). The surface energy balance at Panda 1 Station, Princess Elizabeth Land: A typical katabatic wind region in East Antarctica. Journal of Geophysical Research: Atmospheres, 125, e2019JD030378. https://doi.org/10.1029/2019JD030378.

Fausto, R. S., Box, J. E., Vandecrux, B., van As, D., Steffen, K., MacFerrin, M., Machguth, H., Colgan, W., Koenig, L. S., McGrath, D., Charalampidis, C., & Braithwaite, R. J. (2018). A snow density dataset for improving surface boundary conditions in Greenland ice sheet firn modelling. *Frontiers in Earth Science*, 6(51). https://doi.org/10.3389/feart.2018.00051

Flanner, M. G., & Zender, C. S. (2006). Linking snowpack microphysics and albedo evolution. Journal of Geophysical Research-Atmospheres, 111(D12208), doi:10.1029/2005JD006834. http://internal-pdf//Flanner, 2006. JGR. v111-4182110721/Flanner, 2006. JGR. v111.pdf

Foken T. (2008). Micrometeorology . Berlin: Springer.

Forster, R. R., Box, J. E., van den Broeke, M. R., Miège, C., Burgess, E. W., van Angelen, J. H., Lenaerts, J. T. M., Koenig, L. S., Paden, J., Lewis, C., Gogineni, S. P., Leuschen, C., & McConnell, J. R. (2014). Extensive liquid meltwater storage in firn within the Greenland ice sheet. Nature Geoscience, 7(2), 95–98. https://doi.org/10.1038/ngeo2043

Gardner, A. S. and M. J. Sharp, 2010: A review of snow and ice albedo and the development of a new physically based broadband albedo parameterization. Journal of geophysical research, 115 (F1), F01 009.

Gardner, A. S. (2022). Glacier Energy and Mass Balance - MATLAB (v0.1). Zenodo. https://doi.org/10.5281/zenodo.6975252

Greuell, W., and Konzelmann, T., 1994: Numerical modelling of the energy balance and the englacial temperature of the Greenland Ice Sheet. Calculations for the ETH-Camp location (West Greenland, 1155 m a.s.l.). Global and Planetary Change, 9: 91–114.

Greuell, W., & Oerlemans, J. (1989). The Evolution of the Englacial Temperature Distribution in the Superimposed Ice Zone of a Polar Ice Cap During a Summer Season BT - Glacier Fluctuations and Climatic Change (J. Oerlemans (Ed.); pp. 289–303). Springer Netherlands.

Guyomarc'h, G. and Merindol, L. (1998) Validation of an application for forecasting blowing snow, Ann. Glaciol., 26, 138–143.

https://doi.org/10.5194/egusphere-2022-674
Preprint. Discussion started: 16 August 2022

Helsen, M. M., M. R. van den Broeke, R. S. W. van de Wal, W. J. van de Berg, E. van Meijgaard, C. H. Davis, Y. Li, and I. Goodwin, 2008: Elevation changes in Antarctica mainly determined by accumulation variability, *Science*, 320, 1626– 1629, doi:10.1126/science.1153894.

Herron, M., and Langway, C. (1980). Firn Densification: An Empirical Model. Journal of Glaciology, 25(93), 373-385. doi:10.3189/S0022143000015239.

Hirashima, H., Avanzi, F., & Yamaguchi, S. (2017). Liquid water infiltration into a layered snowpack: evaluation of a 3-D water transport model with laboratory experiments. Hydrol. Earth Syst. Sci., 21(11), 5503–5515. https://doi.org/10.5194/hess-21-5503-2017

Högström U. (1996). Review of some basic characteristics of the atmospheric surface layer. Boundary-Layer Meteorology 78,215246.

Horlings, A. N., Christianson, K., Holschuh, N., Stevens, C. M., & Waddington, E. D. (2021). Effect of horizontal divergence on estimates of firn-air content. Journal of Glaciology, 67(262), 287–296. https://doi.org/DOI: 10.1017/jog.2020.105

Janssens, I., & Huybrechts, P. (2000). The treatment of meltwater retention in mass-balance parameterizations of the Greenland ice sheet. Annals of Glaciology, 31, 133–140. https://doi.org/DOI: 10.3189/172756400781819941

Kaspers, K. A., van de Wal, R. S. W., van den Broeke, M. R., Schwander, J., van Lipzig, N. P. M., and Brenninkmeijer, C. A. M.: Model calculations of the age of firn air across the Antarctic continent, Atmos. Chem. Phys., 4, 1365–1380, https://doi.org/10.5194/acp-4-1365-2004, 2004.

Kuipers Munneke, P., Ligtenberg, S. R. M., Noël, B. P. Y., Howat, I. M., Box, J. E., Mosley-Thompson, E., McConnell, J. R., Steffen, K., Harper, J. T., Das, S. B., and van den Broeke, M. R., 2015: Elevation change of the Greenland Ice Sheet due to surface mass balance and firn processes, 1960–2014, The Cryosphere, 9, 2009–2025, https://doi.org/10.5194/tc-9-2009-2015.

Larour, E., M. Morlighem, H. Seroussi, J. Schiermeier and E. Rignot, 2012a, Ice flow sensitivity to geothermal heat flux of Pine Island Glacier, Antarctica, J. Geophys. Res., 117, F04023, doi:10.1029/2012JF002371.

Larour, E., J. Schiermeier, E. Rignot, H. Seroussi, and M. Morlighem, 2012b, Sensitivity Analysis of Pine Island Glacier ice flow using ISSM and DAKOTA, J. Geophys. Res., 117, F02009, doi:10.1029/2011JF002146.

Lefebre, F., H. Galle´e, J.-P. van Ypersele, and W. Greuell, 2003: Modeling of snow and ice melt at ETH Camp (West Greenland): A study of surface albedo, J. Geophys. Res., 108(D8), 4231, doi:10.1029/2001JD001160.

Lenaerts, J. T. M., van den Broeke, M. R., Déry, S. J., König-Langlo, G., Ettema, J., & Munneke, P. K. (2010). Modelling snowdrift sublimation on an Antarctic ice shelf. The Cryosphere, 4(2), 179–190. https://doi.org/10.5194/tc-4-179-2010,

Li, J., & Zwally, H., 2004: Modeling the density variation in the shallow firn layer. *Annals of Glaciology, 38*, 309-313. doi:10.3189/172756404781814988.

https://doi.org/10.5194/egusphere-2022-674
Preprint. Discussion started: 16 August 2022

Ligtenberg, S. R. M., Helsen, M. M., and van den Broeke, M. R., 2011: An improved semi-empirical model for the densification of Antarctic firn. The Cryosphere, 5(4), 809–819. https://doi.org/10.5194/tc-5-809-2011

Ligtenberg, S. R. M., Kuipers Munneke, P., Noël, B. P. Y., and van den Broeke, M. R.: Brief communication: Improved simulation of the present-day Greenland firn layer (1960–2016), The Cryosphere, 12, 1643–1649, https://doi.org/10.5194/tc-12-1643-2018, 2018.

Liston, G. E., & Elder, K. (2006). A Distributed Snow-Evolution Modeling System (SnowModel). Journal of Hydrometeorology, 7(6), 1259–1276. https://doi.org/10.1175/JHM548.1

Lundin, J. M. D., Stevens, C. M., Arthern, R., Buizert, C., Orsi, A., Ligtenberg, S. R. M., Simonsen, S. B., Cummings, E., Essery, R., Leahy, W., Harris, P., Helsen, M. M., & Waddington, E. D. (2017). Firn Model Intercomparison Experiment (FirnMICE). Journal of Glaciology, 63(239), 401–422. https://doi.org/10.1017/jog.2016.114

Marbouty, D., 1980: An experimental study of temperature-gradient metamorphism. Journal of Glaciology, 26, 303-312.

Male, D. H., & Granger, R. J. (1981). Snow surface energy exchange. Water Resources Research, 17(3), 609–627. file:///E:/Work_Computer/Articles/Articles/Male, 1981. Water Resources Research. V17.pdf

Marsh, P., & Woo, M.K. (1984). Wetting front advance and freezing of meltwater within a snow cover: 2. A simulation model. Water Resources Research, 20(12), 1865–1874. https://doi.org/https://doi.org/10.1029/WR020i012p01865

Marchenko, S., van Pelt, W. J. J., Claremar, B., Pohjola, V., Pettersson, R., Machguth, H., & Reijmer, C. (2017). Parameterizing Deep Water Percolation Improves Subsurface Temperature Simulations by a Multilayer Firn Model . In Frontiers in Earth Science (Vol. 5, p. 16). https://www.frontiersin.org/article/10.3389/feart.2017.00016

Medley, B., Neumann, T. A., Zwally, H. J., and Smith, B. E.: Forty-year Simulations of Firn Processes over the Greenland and Antarctic Ice Sheets, The Cryosphere Discuss. [preprint], https://doi.org/10.5194/tc-2020-266, in review, 2020.

Miller, N. B., Shupe, M. D., Cox, C. J., Noone, D., Persson, P. O. G., and Steffen, K.: Surface energy budget responses to radiative forcing at Summit, Greenland, The Cryosphere, 11, 497–516, https://doi.org/10.5194/tc-11-497-2017, 2017.

Montgomery, L., L. Koenig, and P. Alexander, 2018: The SUMup dataset: Compiled measurements of surface mass balance components over ice sheets and sea ice with analysis over Greenland. Earth Syst. Sci. Data, 10, 1959-1985, doi:10.5194/essd-10-1959-2018.

Munro, D. S., & Davies, J. A. (1977). An experimental study of the glacier boundary layer over melting ice. Journal of Glaciology, 18(80), 425–436. https://doi.org/DOI: 10.3189/S0022143000021109

Murphy, D.M. and Koop, T., 2005: Review of the Vapour Pressures of Ice and Supercooled Water for Atmospheric Applications. Quarterly Journal of the Royal Meteorological Society, 131, 1539-1565. http://dx.doi.org/10.1256/qj.04.94

https://doi.org/10.5194/egusphere-2022-674
Preprint. Discussion started: 16 August 2022

Murray, F. W. (1967). "On the Computation of Saturation Vapor Pressure." *J. Appl. Meteor.* 6 (1): 203–4. https://doi.org/10.1175/1520-0450(1967)006%3C0203:OTCOSV%3E2.0.CO;2.

Noël, B., van de Berg, W. J., Machguth, H., Lhermitte, S., Howat, I., Fettweis, X., & van den Broeke, M. R. (2016). A daily, 1 km resolution data set of downscaled Greenland ice sheet surface mass balance (1958–2015). The Cryosphere, 10(5), 2361–2377. https://doi.org/10.5194/tc-10-2361-2016

Paterson, W., 1994: The Physics of Glaciers, 3rd ed., Pergamon Press, Oxford, London, New York.

Parish, T. R., & Bromwich, D. H. (1987). The surface windfield over the Antarctic ice sheets. *Nature*, *328*(6125), 51–54. https://doi.org/10.1038/328051a0

Pfeffer, W. T., Illangasekare, T. H., & Meier, M. F. (1990). Analysis and Modeling of Melt-Water Refreezing in Dry Snow. Journal of Glaciology, 36(123), 238–246. https://doi.org/DOI: 10.3189/S0022143000009497

Pfeffer, W. T., Meier, M. F., & Illangasekare, T. H. (1991). Retention of Greenland Runoff by Refreezing - Implications for Projected Future Sea-Level Change. Journal of Geophysical Research-Oceans, 96(C12), 22117–22124. http://internal-pdf//Pfeffer, 1991. JGR. v96-1317438466/Pfeffer, 1991. JGR. v96.pdf

Schlegel, N-J., E Larour, H Seroussi, M. Morlighem, and J. E. Box, 2013, Decadal-scale sensitivity of northeast Greenland ice flow to errors in surface mass balance using ISSM J. Geophys. Res. - Earth Surface, 118, doi: 10.1002/jgrf.20062.

Schlegel, N.-J., E. Larour, H. Seroussi, M. Morlighem and J.E. Box, 2015, Ice discharge uncertainties in Northeast Greenland from boundary conditions and climate forcing of an ice flow model, J. Geophys. Res., 120, 29-54, doi:10.1002/2014JF003359.

Schlegel, N-J. and E. Y. Larour, 2019, Quantification of surface forcing requirements for a Greenland Ice Sheet model using uncertainty analyses. Geophys. Res. Lett., 46. https://doi.org/10.1029/2019GL083532.

Schlegel, N.J., Gardner, A., & Larour, E. (2022). Output from the Glacier Energy and Mass Balance (GEMB v1.0) forced with 3-hourly RACMO fields, Greenland and Antarctica 1979-2014 (1.0) [Data set]. Zenodo. https://doi.org/10.5281/zenodo.6864587

Schaaf, C., Z. Wang. *MCD43C3 MODIS/Terra+Aqua BRDF/Albedo Albedo Daily L3 Global 0.05Deg CMG V006*. 2015, distributed by NASA EOSDIS Land Processes DAAC, https://doi.org/10.5067/MODIS/MCD43C3.006. Accessed 2020-03-19.

Smith B, Fricker HA, Gardner AS, Medley B, Nilsson J, Paolo FS, Holschuh N, Adusumilli S, Brunt K, Csatho B, Harbeck K, Markus T, Neumann T, Siegfried MR, Zwally HJ, 2020: Pervasive ice sheet mass loss reflects competing ocean and atmosphere processes. Science. 2020 Jun 12;368(6496):1239-1242. doi: 10.1126/science.aaz5845. Epub 2020 Apr 30. PMID: 32354841.

https://doi.org/10.5194/egusphere-2022-674
Preprint. Discussion started: 16 August 2022

Sjöblom, A. (2014). Turbulent fluxes of momentum and heat over land in the High-Arctic summer: the influence of observation techniques. *Polar Research*, *33*. https://doi.org/10.3402/polar.v33.21567

Steger, C. R., Reijmer, C. H., van den Broeke, M. R., Wever, N., Forster, R. R., Koenig, L. S., Kuipers Munneke, P., Lehning, M., Lhermitte, S., Ligtenberg, S. R. M., Miège, C., & Noël, B. P. Y. (2017). Firn Meltwater Retention on the Greenland Ice Sheet: A Model Comparison . In Frontiers in Earth Science (Vol. 5, p. 3). https://www.frontiersin.org/article/10.3389/feart.2017.00003

Stevens, C. M., Verjans, V., Lundin, J. M. D., Kahle, E. C., Horlings, A. N., Horlings, B. I., & Waddington, E. D. (2020). The Community Firn Model (CFM) v1.0. Geosci. Model Dev., 13(9), 4355–4377. https://doi.org/10.5194/gmd-13-4355-2020

Sturm, M., J. Holmgren, M. König, and K. Morris, 1997: The thermal conductivity of seasonal snow, J. Glaciol., 43, 26–41.

Tennant, W. (2004). Considerations when using pre-1979 NCEP/NCAR reanalyses in the southern hemisphere. Geophysical Research Letters, 31(11). https://doi.org/https://doi.org/10.1029/2004GL019751

van Angelen, J. H., Lenaerts, J. T. M., van den Broeke, M. R., Fettweis, X., & van Meijgaard, E. (2013). Rapid loss of firn pore space accelerates 21st century Greenland mass loss. Geophysical Research Letters, n/a-n/a. https://doi.org/10.1002/grl.50490

van den Broeke, M. R., Duynkerke, P. G., & Henneken, E. A. C. (1994). Heat, momentum and moisture budgets of the katabatic layer over the melting zone of the West Greenland Ice Sheet in summer. Boundary-Layer Meteorology, 71(4), 393–413.

Vandecrux, B., Mottram, R., Langen, P. L., Fausto, R. S., Olesen, M., Stevens, C. M., Verjans, V., Leeson, A., Ligtenberg, S., Kuipers Munneke, P., Marchenko, S., van Pelt, W., Meyer, C. R., Simonsen, S. B., Heilig, A., Samimi, S., Marshall, S., Machguth, H., MacFerrin, M., … Box, J. E. (2020). The firn meltwater Retention Model Intercomparison Project (RetMIP): evaluation of nine firn models at four weather station sites on the Greenland ice sheet. The Cryosphere, 14(11), 3785–3810. https://doi.org/10.5194/tc-14-3785-2020

van Wessem, J. M., van de Berg, W. J., Noël, B. P. Y., van Meijgaard, E., Amory, C., Birnbaum, G., Jakobs, C. L., Krüger, K., Lenaerts, J. T. M., Lhermitte, S., Ligtenberg, S. R. M., Medley, B., Reijmer, C. H., van Tricht, K., Trusel, L. D., van Ulft, L. H., Wouters, B., Wuite, J., and van den Broeke, M. R. 2018: Modelling the climate and surface mass balance of polar ice sheets using RACMO2 – Part 2: Antarctica (1979–2016), The Cryosphere, 12, 1479–1498, https://doi.org/10.5194/tc-12-1479-2018.

Vandecrux, B., MacFerrin, M., Machguth, H., Colgan, W. T., van As, D., Heilig, A., Stevens, C. M., Charalampidis, C., Fausto, R. S., Morris, E. M., Mosley-Thompson, E., Koenig, L., Montgomery, L. N., Miège, C., Simonsen, S. B., Ingeman-Nielsen, T., & Box, J. E. (2019). Firn data compilation reveals widespread decrease of firn air content in western Greenland. The Cryosphere, 13(3), 845–859. https://doi.org/10.5194/tc-13-845-2019

https://doi.org/10.5194/egusphere-2022-674
Preprint. Discussion started: 16 August 2022

Van Der Veen, C. J. (1993). Interpretation of short-term ice-sheet elevation changes inferred from satellite altimetry. Climatic Change, 23(4), 383–405. https://doi.org/10.1007/BF01091624

Vionnet, V., Brun, E., Morin, S., Boone, A., Faroux, S., Le Moigne, P., Martin, E., and Willemet, J.-M., 2012: The detailed snowpack scheme Crocus and its implementation in SURFEX v7.2, Geosci. Model Dev., 5, 773–791, https://doi.org/10.5194/gmd-5-773-2012.

Warren, S. G., & Wiscombe, W. J. (1980). A model for the spectral albedo of snow. II: Snow containing atmospheric aerosols. Journal of the Atmospheric Sciences, 37(12), 2734–2745. 1980. J. Atmospheric Sciences. v37.pdf

Weinhart, A. H., Freitag, J., Hörhold, M., Kipfstuhl, S., and Eisen, O.: Representative surface snow density on the East Antarctic Plateau, The Cryosphere, 14, 3663–3685, https://doi.org/10.5194/tc-14-3663-2020, 2020.

Wiscombe, W. J., & Warren, S. G. (1980). A model for the spectral albedo of snow. I: Pure snow. Journal of the Atmospheric Sciences, 37(12), 2712–2733. file:///E:/Work_Computer/Articles/Articles/Wiscombe, 1980. J. Atmospheric Sciences. V37.pdf

Zwally, H. J. A. Y., Bindschadler, R. A., Brenner, A. C., Major, J. A., & Marsh, J. G. (1989). Growth of Greenland Ice Sheet: Measurement. Science, 246(4937), 1587 LP – 1589. https://doi.org/10.1126/science.246.4937.1587

Zwally, H. J., Giovinetto, M. B., Li, J., Cornejo, H. G., Beckley, M. A., Brenner, A. C., Saba, J. L., & Yi, D. (2005). Mass changes of the Greenland and Antarctic ice sheets and shelves and contributions to sea-level rise: 1992–2002. Journal of Glaciology, 51(175), 509–527. https://doi.org/DOI: 10.3189/172756505781829007

https://doi.org/10.5194/egusphere-2022-674
Preprint. Discussion started: 16 August 2022

Tables

Table 1: GEMB model parameters used in this study

Parameter	Greenland	Antarctic
dz_{top}	0.05 m	0.05 m
dz_{min}	0.025 m	0.025 m
z_{top}	10 m	10 m
z_{max}	250 m	250 m
z_{min}	130 m	130 m
Thermal conductivity	Sturm et al., 1997	Strum, 1997
Albedo	Gardner and Sharp, 2009 $d\alpha_c$, $d\alpha_u$, $d\alpha_\tau$ set to zero	Gardner and Sharp, 2009 $d\alpha_c$, $d\alpha_u$, $d\alpha_\tau$ set to zero
Bare ice albedo	MODIS MCD43C3	MODIS MCD43C3
SW subsurface absorption	No	No
Compaction	Arthern et al. (2010)	Arthern et al. (2010)
Compaction calibration	Kuipers Munneke et al. (2015) $b_{550/830}$ = *1.27/2.00* $m_{550/830}$ = *-0.12/-0.25* $r^2_{550/830}$ = 0.18/0.92	Ligtenberg et al. (2011) $b_{550/830}$ = *1.64/2.00* $m_{550/830}$ = *-0.17/-0.24* $r^2_{550/830}$ = 0.28/0.55
Falling snow density	315 kg/m^3 (Fausto et al., 2018)	function of the annual temperature, accumulation, surface pressure and wind speed (Kaspers et al. 2004)
Spinup	~5000 years Climatology 1979-1988	~6000 years Climatology 1979-1999

855

https://doi.org/10.5194/egusphere-2022-674
Preprint. Discussion started: 16 August 2022

Figures

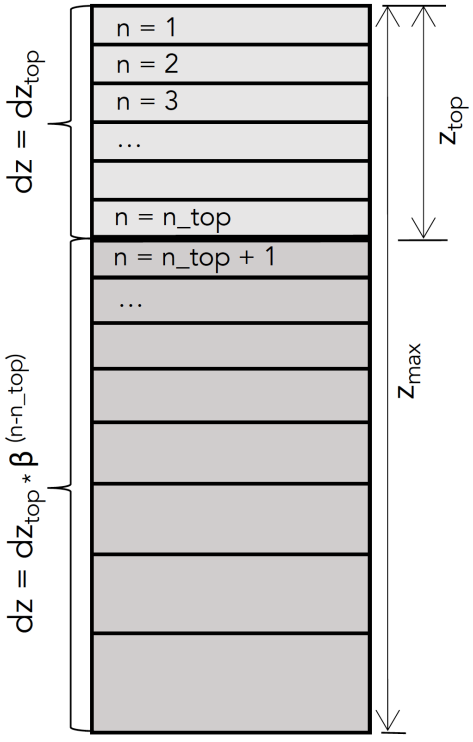

Figure 1: Diagram showing the model layer initialization as described in Section 2.1. *dz* is the layer thickness, dz_{top} is the maximum near-surface thickness, z_{top} is the depth of the near-surface, z_{max} is the maximum column depth, β is a unitless scaling by depth parameter, and *n* is the layer number.

https://doi.org/10.5194/egusphere-2022-674
Preprint. Discussion started: 16 August 2022

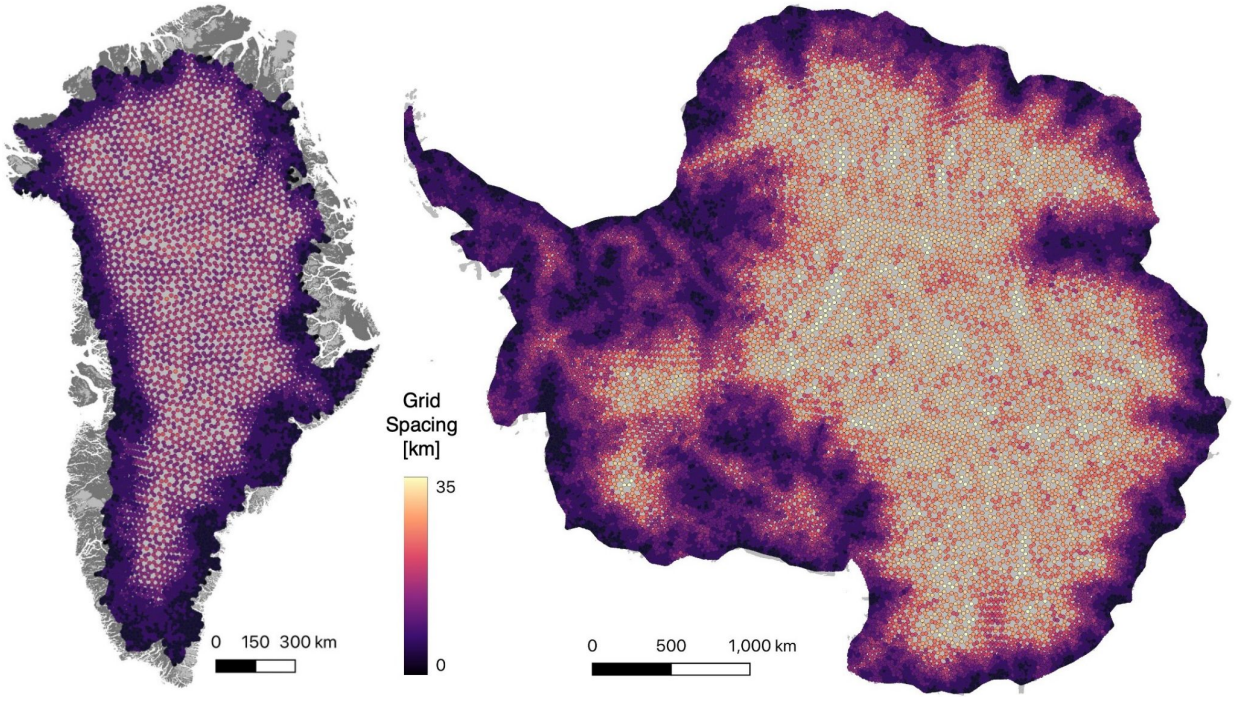

Figure 2: GEMB Greenland (left) and Antarctic (right) model grids used for this study.

https://doi.org/10.5194/egusphere-2022-674
Preprint. Discussion started: 16 August 2022

865

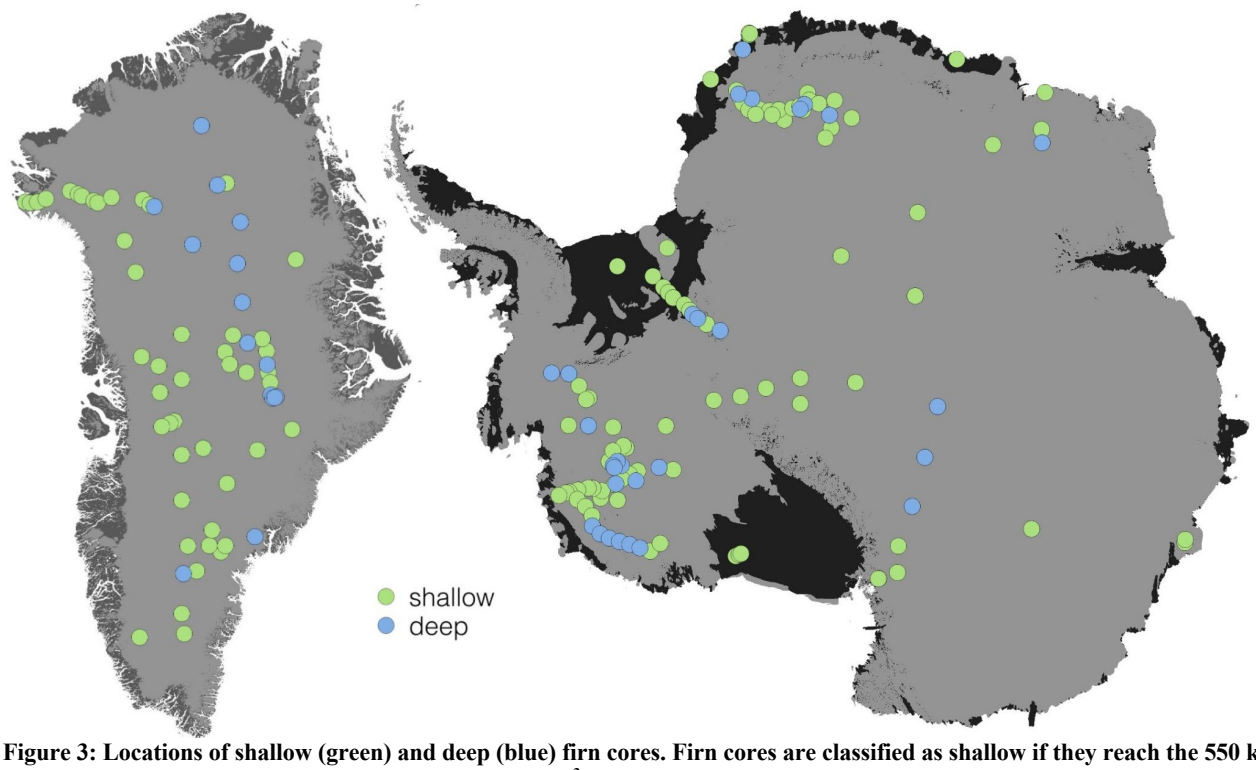

Figure 3: Locations of shallow (green) and deep (blue) firn cores. Firn cores are classified as shallow if they reach the 550 kg m^{-3} density horizon and deep if they extend to the 830 kg m^{-3} density horizon.

https://doi.org/10.5194/egusphere-2022-674
Preprint. Discussion started: 16 August 2022

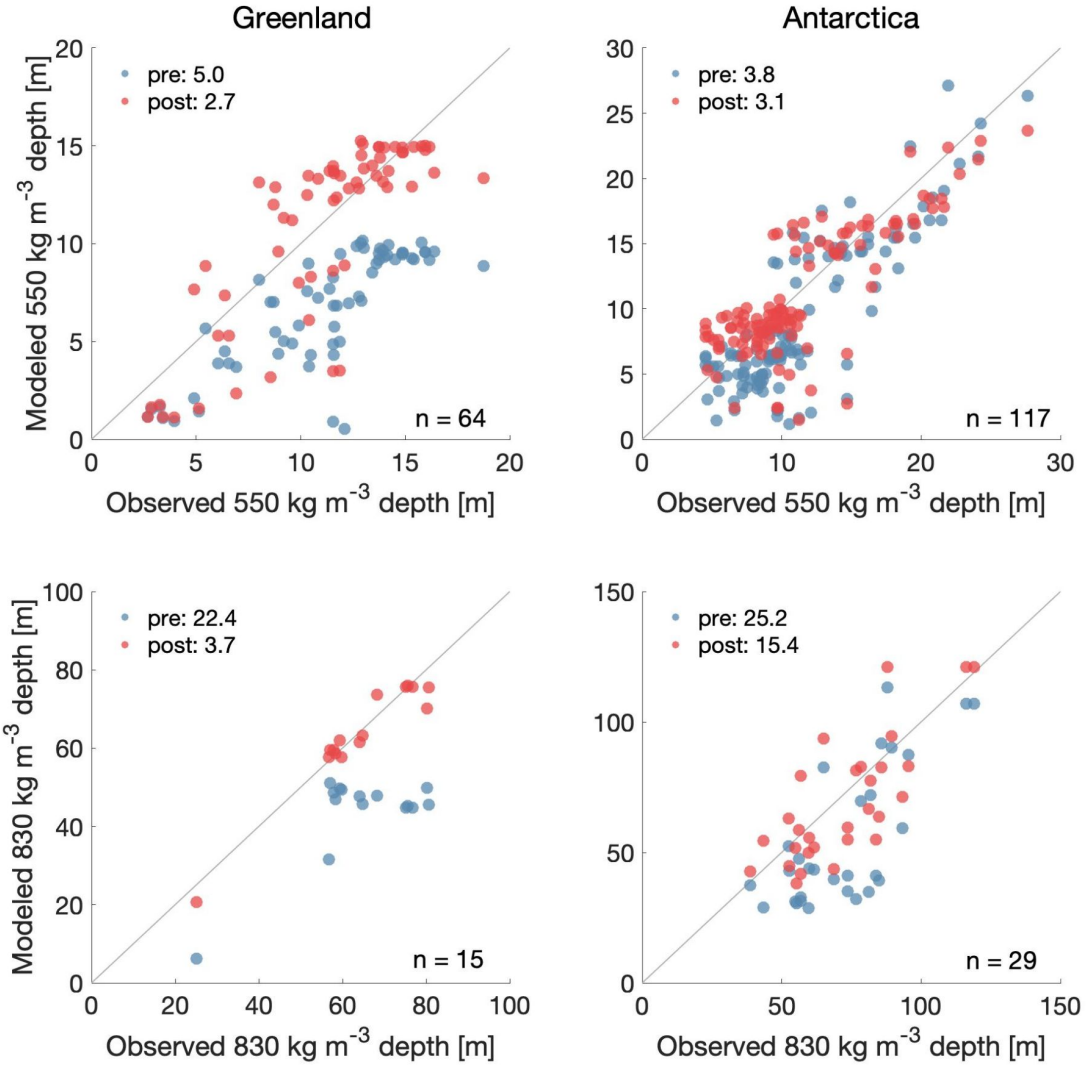

Figure 4: Comparison between modeled and observed 550 kg m^{-3} (top) and 830 kg m^{-3} (bottom) depths for the Greenland (left) and Antarctic (right) Ice Sheets for the locations of firn cores shown in Figure 3. Blue markers show pre-calibrated model agreement with observations, red markers show the post-calibrated model fit. The one-to-one line is shown by the black diagonal lines. Pre and post model calibration fits to observations (RMSE) are show in the top left of each panel.

https://doi.org/10.5194/egusphere-2022-674
Preprint. Discussion started: 16 August 2022

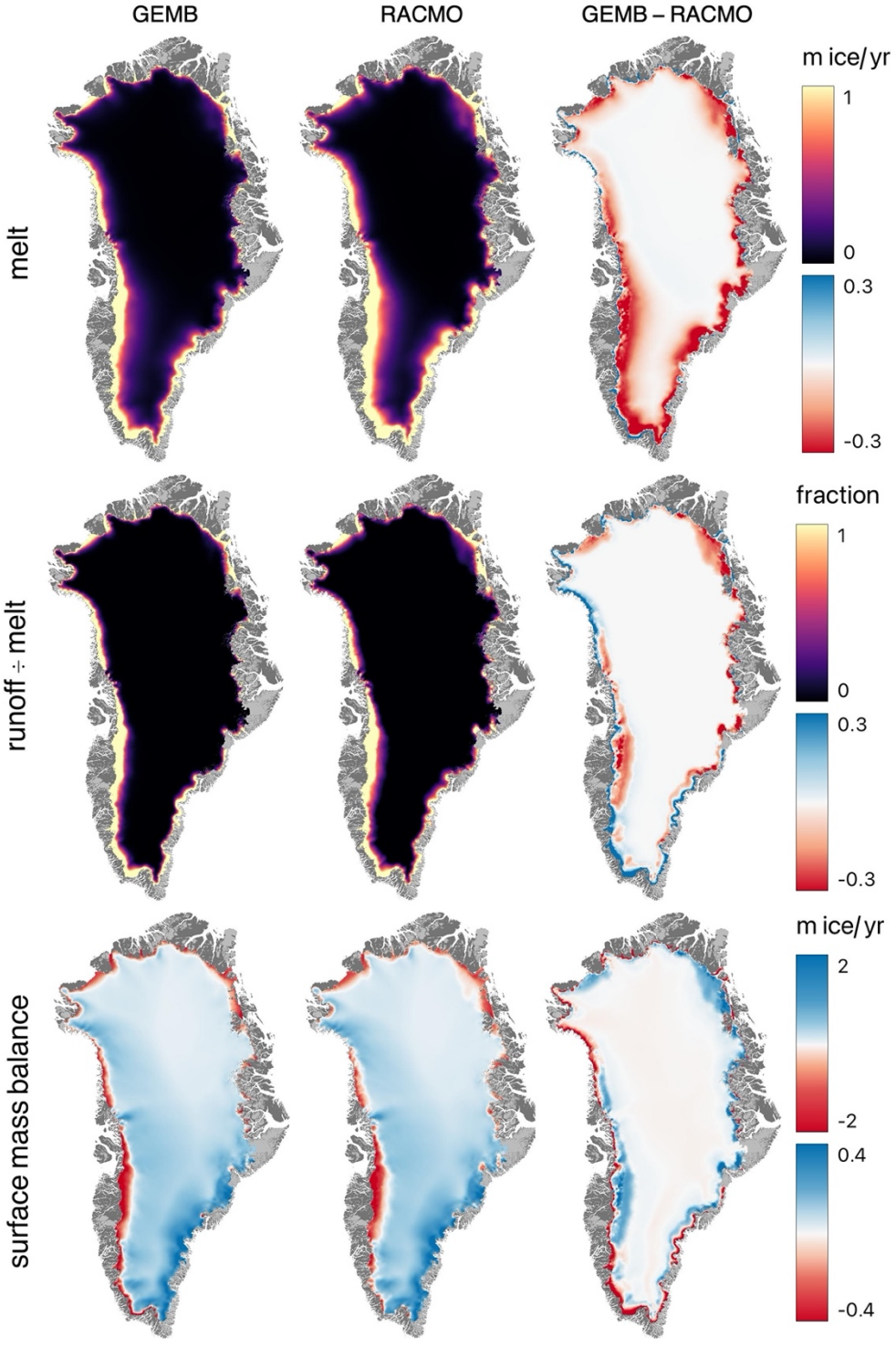

Figure 5: Mean 1979-2014 Greenland Ice Sheet GEMB (left) and RACMO (middle) model output in meters ice equivlent, and their difference (right).

https://doi.org/10.5194/egusphere-2022-674
Preprint. Discussion started: 16 August 2022

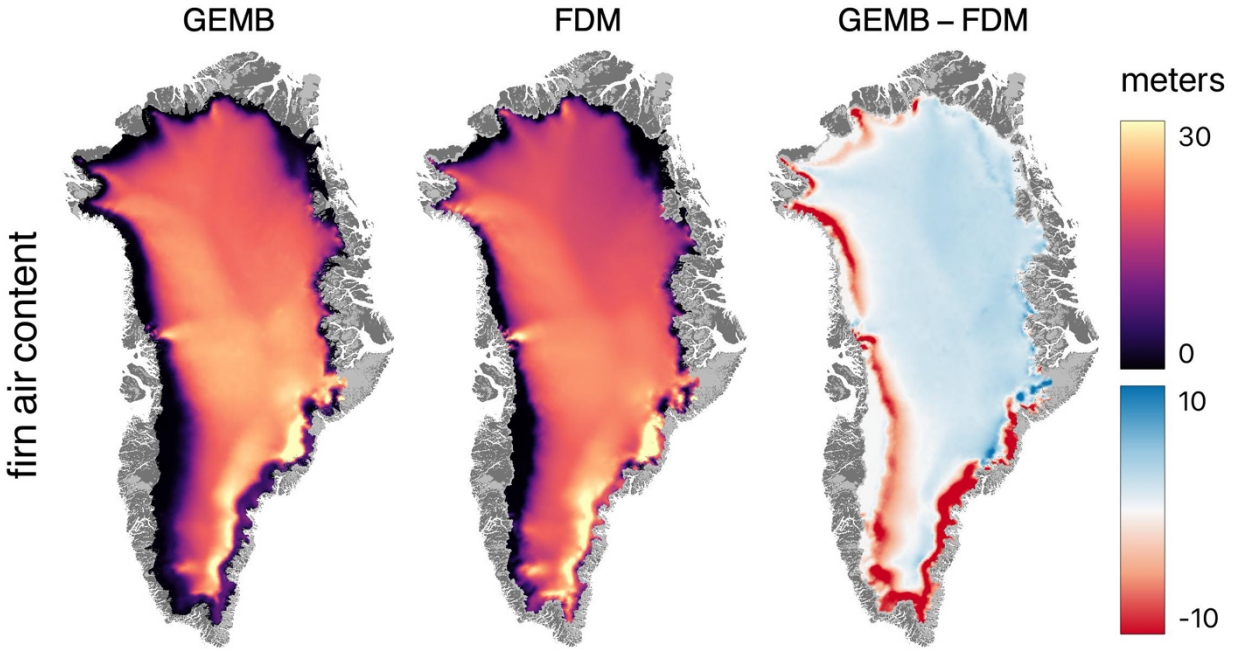

880 **Figure 6: Mean 1979-2014 Greenland Ice Sheet GEMB (left) and IMAU-FDM (middle) firn air content, and their difference (right).**

https://doi.org/10.5194/egusphere-2022-674
Preprint. Discussion started: 16 August 2022

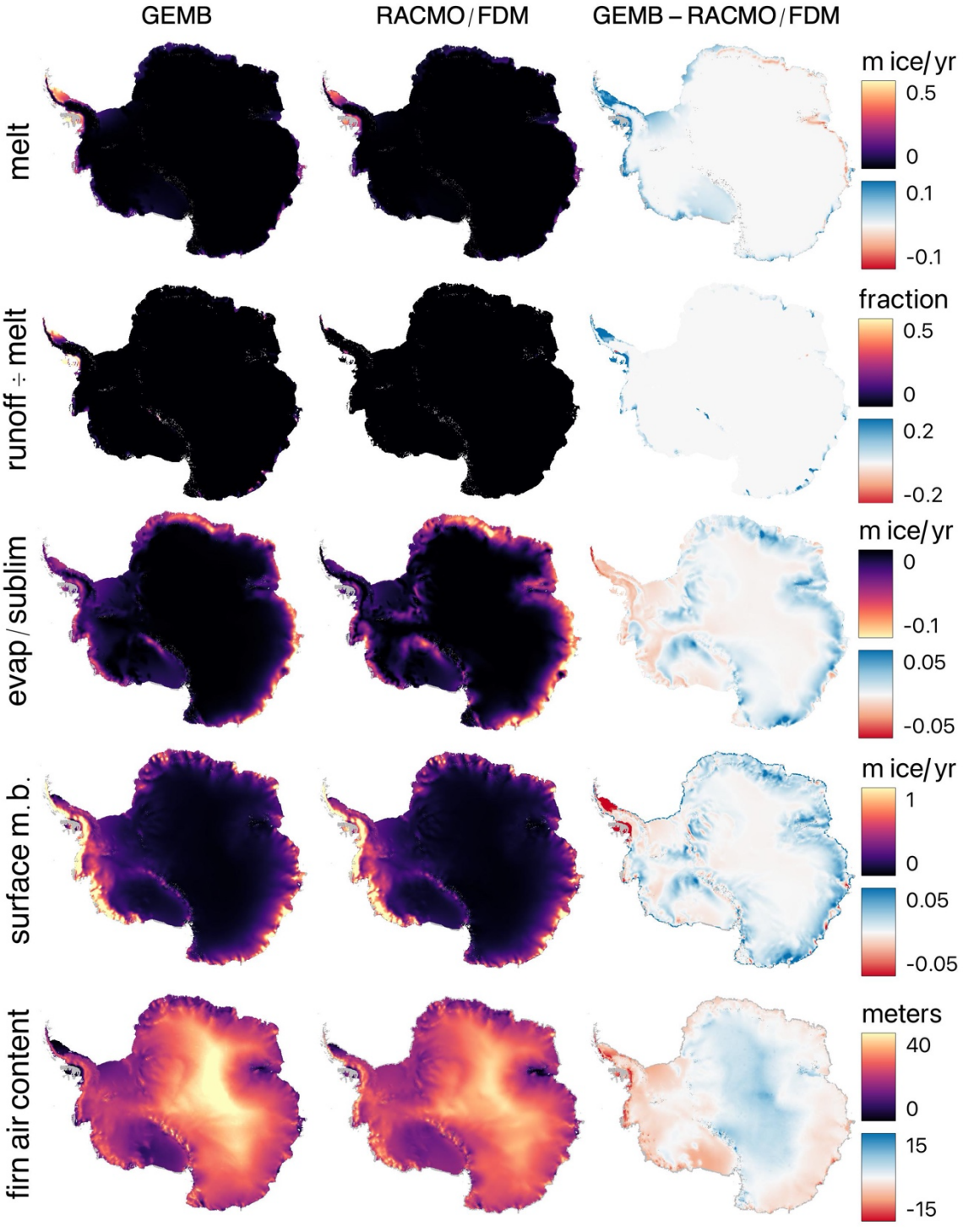

Figure 7: Mean 1979-2014 Antarctic Ice Sheet GEMB (left) and RACMO/FDM (middle) model output in meters ice equivalent units, and their difference (right).

https://doi.org/10.5194/egusphere-2022-674
Preprint. Discussion started: 16 August 2022

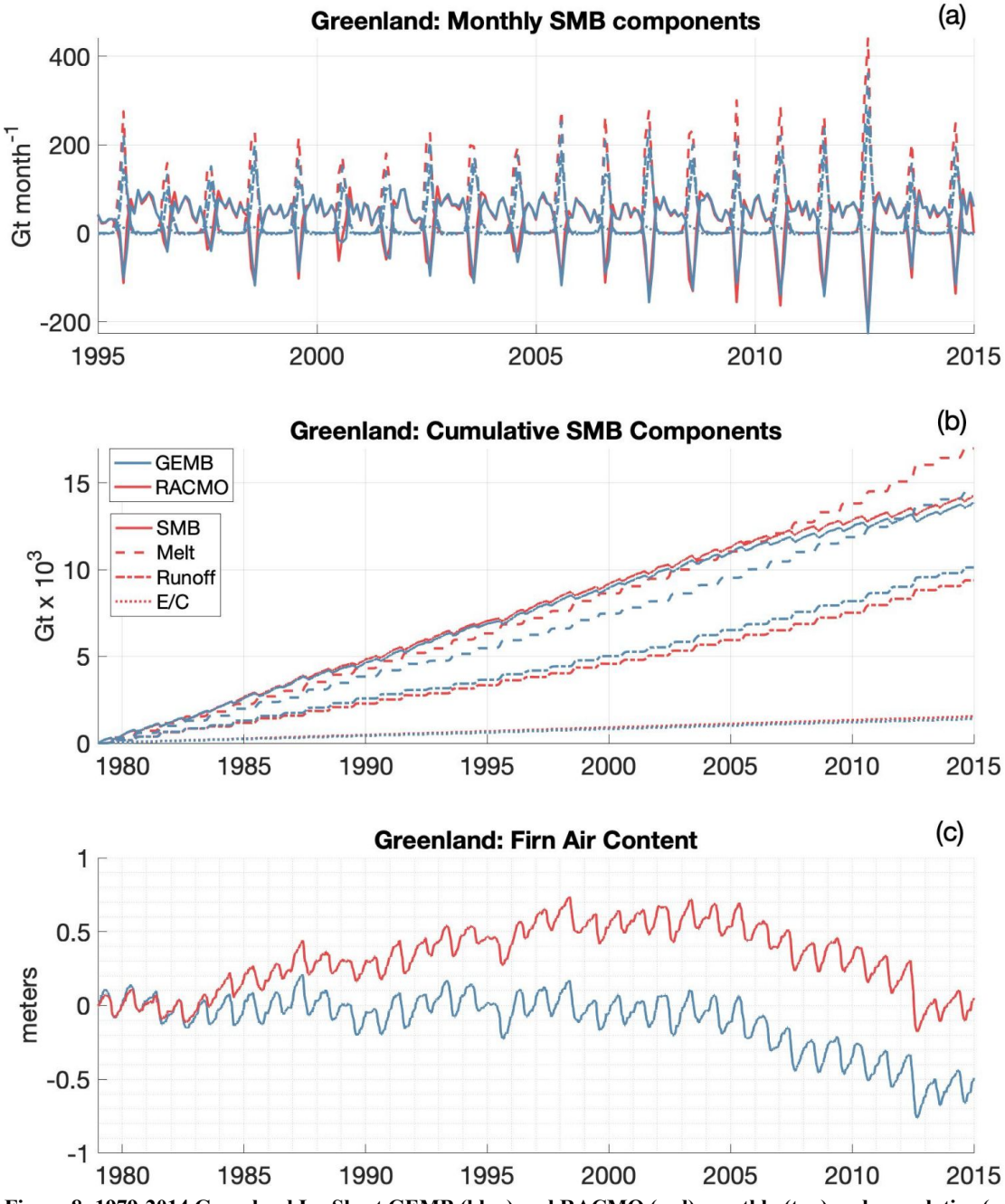

Figure 8: 1979-2014 Greenland Ice Sheet GEMB (blue) and RACMO (red) monthly (top) and cumulative (middle) model output. GEMB and IMAU-FDM average fin air content anomaly, relative to 1979, shown in bottom panel.

https://doi.org/10.5194/egusphere-2022-674
Preprint. Discussion started: 16 August 2022

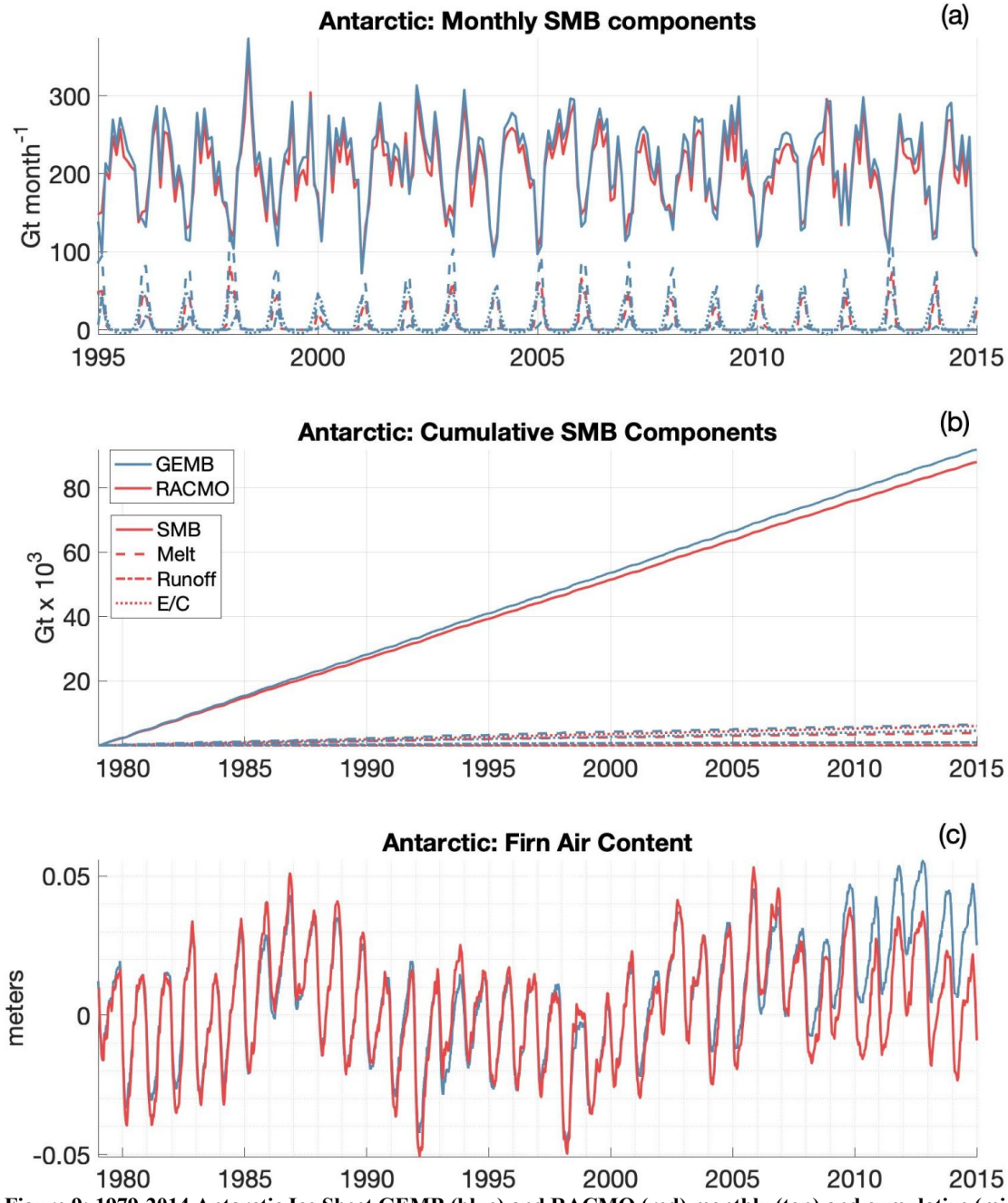

Figure 9: 1979-2014 Antarctic Ice Sheet GEMB (blue) and RACMO (red) monthly (top) and cumulative (middle) model output. GEMB and IMAU-FDM average fin air content anomaly, relative to 1979, shown in bottom panel.

https://doi.org/10.5194/egusphere-2022-674
Preprint. Discussion started: 16 August 2022

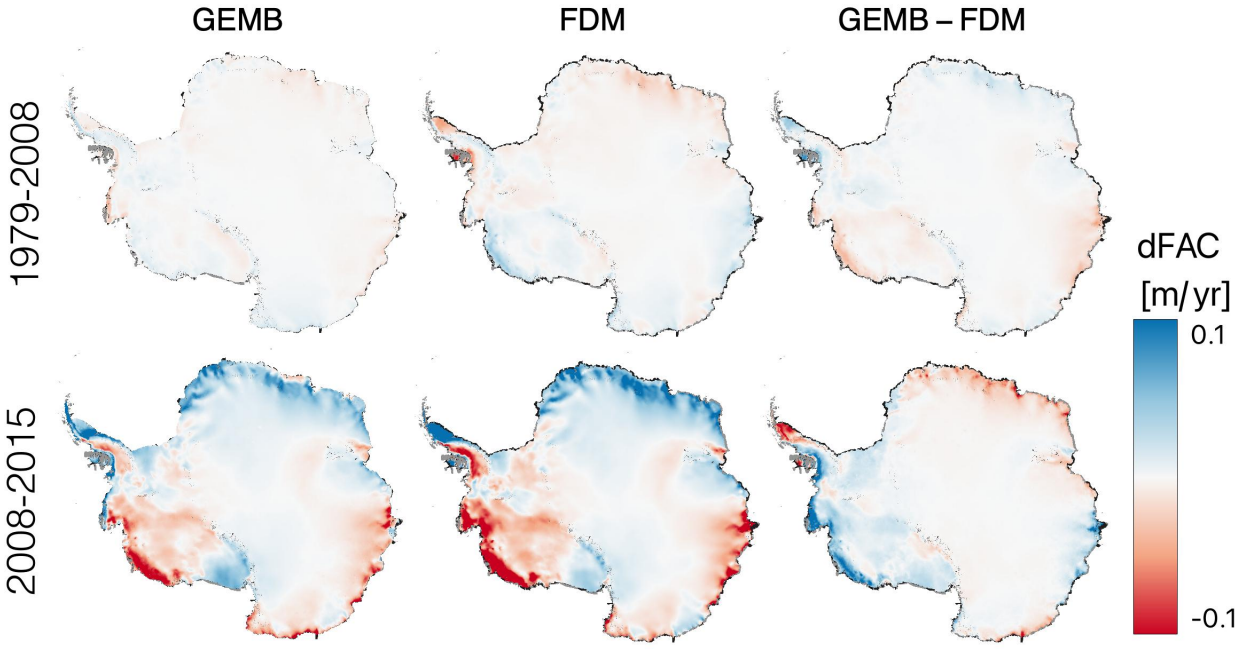

Figure 10: Rate of firn air content change (dFAC) for the Antarctic Ice Sheet as modeled by GEMB (left) and IMAU-FDM (center), and their difference (right). Rates for the period 1979-2008 are shown in the top panels and rates for the 2008-2015 period are shown in the bottom panels.

https://doi.org/10.5194/egusphere-2022-674
Preprint. Discussion started: 16 August 2022

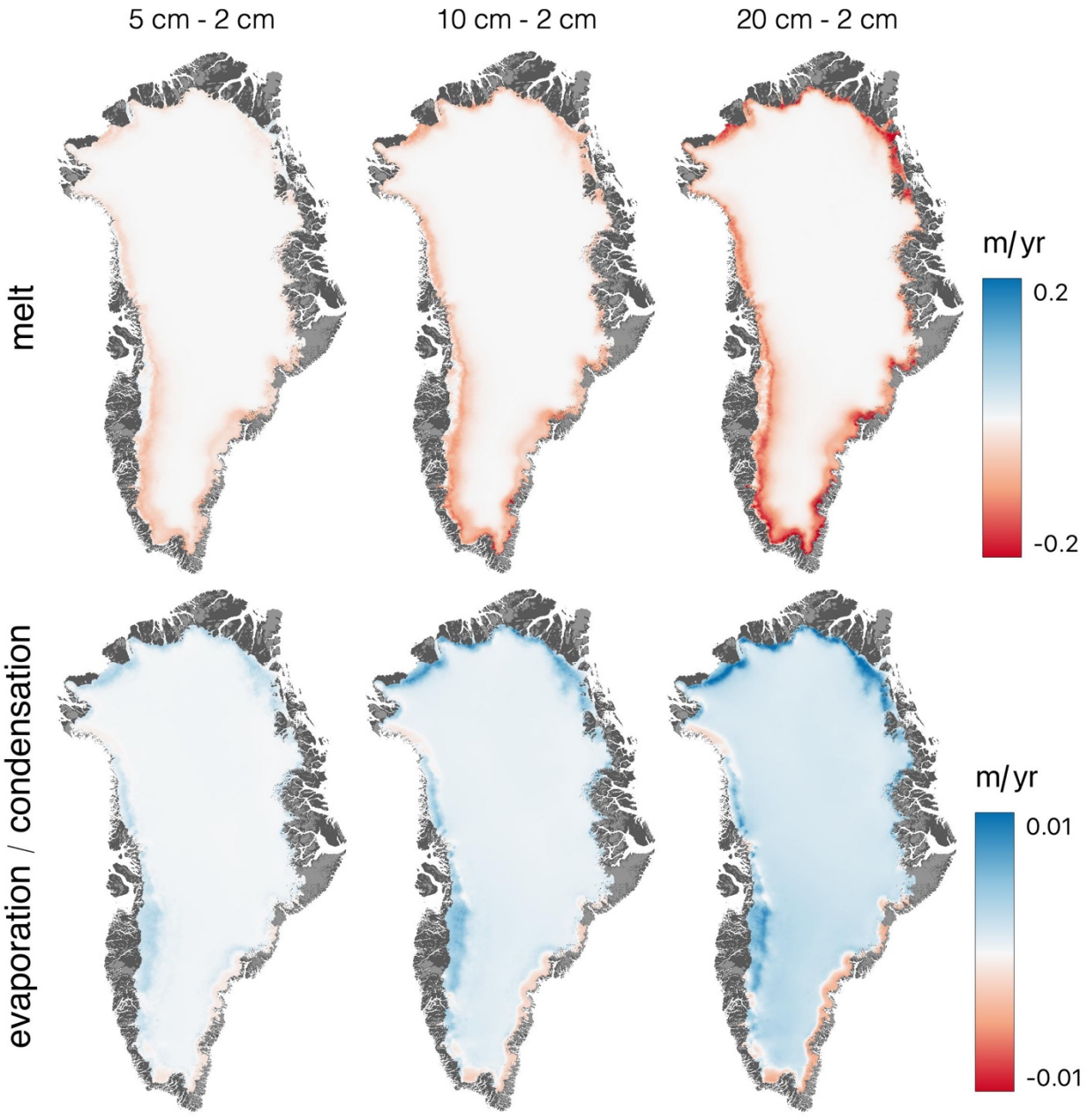

Figure 11: GEMB change in modeled rate of melt (top) and evaporation/condensation (bottom) for near-surface model layer depths (dz_{top}) of 5 cm, 10 cm, and 20 cm, relative to a near-surface model layer depth of 2 cm.

https://doi.org/10.5194/egusphere-2022-674
Preprint. Discussion started: 16 August 2022

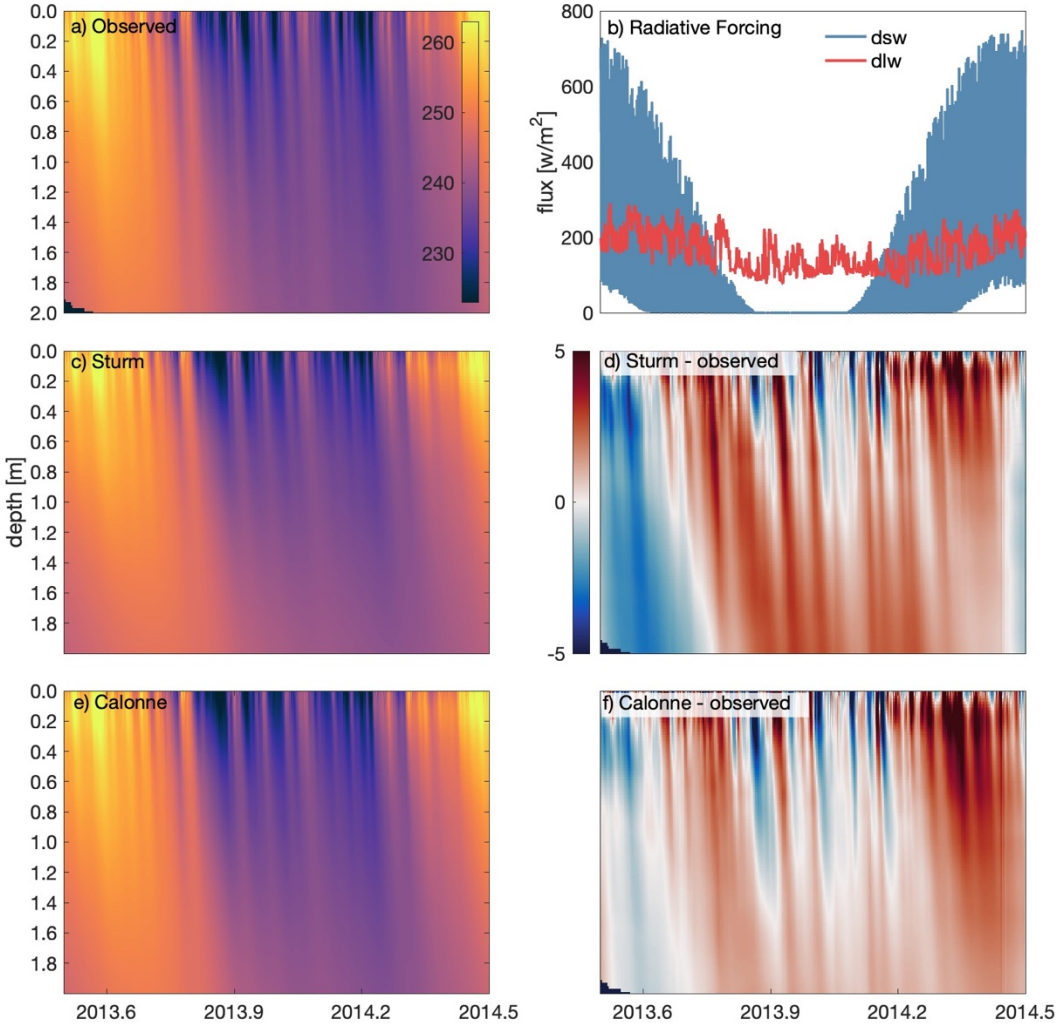

Figure 12: Observed and modeled daily near-surface (upper 2m) temperatures for Summit Station, Greenland (72.580° N and 38.459° W) from July 2013 to June 2014. Temperature profiles from (a) observations (Miller et al., 2017), (c) modeled using GEMB and Sturm et al. (1997) thermal conductivity and (e) modeled using GEMB and Calonne et al. (2011) thermal conductivity. (b) Observed downward shortwave (dsw) and longwave (dlw) radiation provided for context. Differences between temperature profiles for (d) GEMB-Sturm and observation and (f) GEMB-Calonne and observations. Note: All GEMB simulations are forced with RACMO model output (see Table 1) and therefore modeled temperature differences, relative to observations, are due to errors in forcing, model parametrizations and observations.

https://doi.org/10.5194/egusphere-2022-674
Preprint. Discussion started: 16 August 2022

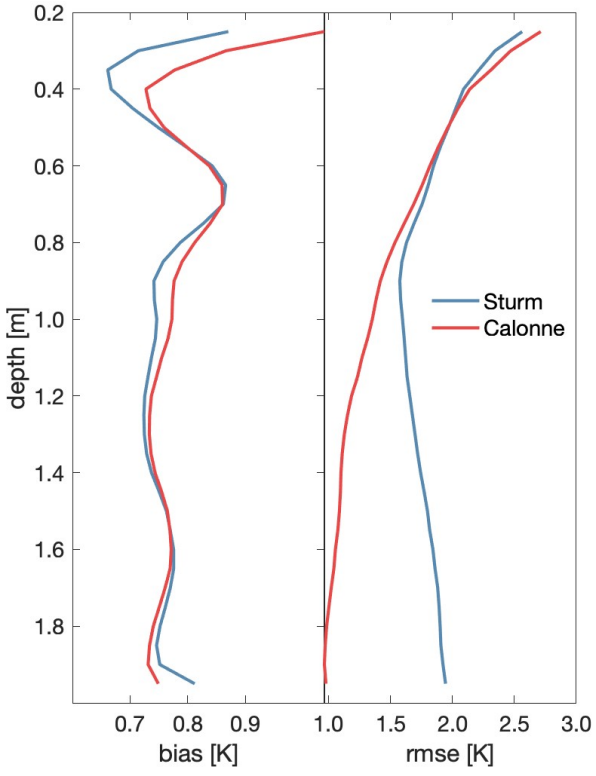

915 **Figure 13: Mean bias (left) and rmse (right) in modeled near-surface temperatures as a function of depth, relative to observations (Miller et al., 2017). Daily GEMB model results using Sturm et al. (1997) and Calonne et al. (2011) thermal conductivity parameterizations for Summit Station, Greenland (72.580° N and 38.459° W) from July 2013 to June 2014.**

920